

## The influence of water-saturation on the strength of volcanic rocks and the stability of lava domes

Michael J. Heap <sup>a,b,\*</sup>, Claire Harnett <sup>c,\*\*</sup>, Jamie Farquharson <sup>d,e</sup>, Patrick Baud <sup>a</sup>, Marina Rosas-Carbajal <sup>f</sup>, Jean-Christophe Komorowski <sup>f</sup>, Marie E.S. Violay <sup>g</sup>, H. Albert Gilg <sup>h</sup>, Thierry Reuschlé <sup>a</sup>

<sup>a</sup> Université de Strasbourg, CNRS, Institut Terre et Environnement de Strasbourg, UMR 7063, 5 rue René Descartes, Strasbourg F-67084, France

<sup>b</sup> Institut Universitaire de France (IUF), Paris, France

<sup>c</sup> School of Earth Sciences, University College Dublin, Dublin, Ireland

<sup>d</sup> Institute for Research Administration, Niigata University, Ikarashi 2-8050, Nishi-ku, Niigata 950-2181, Japan

<sup>e</sup> Research Institute for Natural Hazards and Disaster Recovery, Niigata University, Ikarashi 2-8050, Nishi-ku, Niigata 950-2181, Japan

<sup>f</sup> Université de Paris Cité, Institut de Physique du Globe de Paris, CNRS, F-75005 Paris, France

<sup>g</sup> Laboratory of Experimental Rock Mechanics, Ecole Polytechnique Fédérale de Lausanne, Lausanne, Switzerland

<sup>h</sup> TUM School of Engineering and Design, Technical University of Munich, Arcisstrasse 21, 80333 Munich, Germany

### ARTICLE INFO

#### Keywords:

Hydrothermal alteration  
Uniaxial compressive strength  
Young's modulus  
Fracture toughness  
Dome collapse

### ABSTRACT

The rocks forming a volcanic edifice or dome are typically saturated or partially-saturated with water. However, most experiments aimed at better understanding the mechanical behaviour of volcanic rocks have been performed on dry samples, and therefore most large-scale models designed to explore volcano stability have used parameters representative for dry rock. Here, we present a combined laboratory and modelling study in which we (1) quantified the influence of water-saturation on the mechanical behaviour of variably altered dome rocks from La Soufrière de Guadeloupe (Eastern Caribbean) and (2) used these new data to investigate the influence of water on dome stability. Our laboratory data show that the ratio of wet to dry uniaxial compressive strength (UCS) and Young's modulus are ~0.30–0.95 and ~0.10–1.00, respectively. In other words, the dome rocks were all mechanically weaker when water-saturated. Further, the ratio of wet to dry UCS decreased with increasing alteration (the wt% of secondary minerals in the rocks). Micromechanical modelling suggests that the observed water-weakening is the result of a decrease in fracture toughness ( $K_{IC}$ ) in the presence of water. The ratio of wet to dry  $K_{IC}$  also decreases with increasing alteration, explaining why water-weakening increased as a function of alteration. To explore the influence of water-saturation on lava dome stability, we numerically generated lava domes in Particle Flow Code using the experimental data corresponding to unaltered and altered rock under dry conditions. The strength of the dome-forming rocks was then reduced to values corresponding to wet conditions. Our modelling shows that, although the stability of the unaltered dome was not influenced by water-saturation, larger displacements were observed for the wet altered dome. Additional simulations in which we modelled a buried alteration zone within an otherwise unaltered dome showed that higher displacements were observed when the dome was water-saturated. We conclude that (1) the water-saturation reduces the UCS and Young's modulus of volcanic rock, (2) larger decreases in UCS in the presence of water are observed for altered rocks, and (3) the stability of a dome can be compromised by the presence of water if the dome is altered, or contains an altered zone. These conclusions highlight that the degree of alteration and water-saturation should be mapped and monitored at active volcanoes worldwide, and that large-scale models should use values for water-saturated rocks when appropriate.

\* Corresponding author at: Université de Strasbourg, CNRS, Institut Terre et Environnement de Strasbourg, UMR 7063, 5 rue René Descartes, Strasbourg F-67084, France.

\*\* Corresponding author at: School of Earth Sciences, University College Dublin, Dublin, Ireland.

E-mail addresses: [heap@unistra.fr](mailto:heap@unistra.fr) (M.J. Heap), [claire.harnett@ucd.ie](mailto:claire.harnett@ucd.ie) (C. Harnett).

## 1. Introduction

The short- and long-term strength of rock is influenced not only by pore fluid pressures, but also by the presence of water within the void space (e.g., Baud et al., 2000; Brantut et al., 2013). Based on experiments and micromechanical analyses, reductions to the strength of rock associated with the presence of water are thought to be the result of a decrease in specific surface energy, friction coefficient, and fracture toughness (e.g., Baud et al., 2000; Noël et al., 2021), the presence of clay minerals (e.g., Hawkins and McConnell, 1992; Heap et al., 2019), adsorption pressures (e.g., Risnes et al., 2005), and/or an increase in the efficiency of sub-critical crack growth (e.g., Atkinson, 1984; Kranz et al., 1982; Masuda, 2001; Brantut et al., 2013; Tang et al., 2018).

Although water-weakening (the ratio of wet to dry strength) is reasonably well-documented for sedimentary rocks such as sandstone (e.g., Rutter and Mainprice, 1978; Chester and Logan, 1986; Hawkins and McConnell, 1992; Baud et al., 2000; Duda and Renner, 2013; Wasantha and Ranjith, 2014; Baud et al., 2015; Heap et al., 2019; Noël et al., 2021), carbonate rocks (e.g., Risnes et al., 2005; Baud et al., 2016; Nicolas et al., 2016; Castagna et al., 2018), and gypsum (e.g., Caselle et al., 2022), few data exist for volcanic rocks. For example, the onset of inelastic compaction in tuff from Alban Hills (Italy) was reduced by the presence of water (Zhu et al., 2011). The uniaxial compressive strength of tuffs containing alunite (Heap et al., 2015) and zeolites and clay minerals (Heap et al., 2018) was also lower in the presence of water. Zhu et al. (2016) found that the compressive strength of a basalt from Mt. Etna (Italy) was reduced in the presence of water. Finally, the uniaxial compressive strength and Young's modulus of lava from Mount Unzen (Japan) (Kendrick et al., 2021) and the uniaxial compressive strength of lavas from Mt. Etna, Volvic (France), Kumamoto (Japan), and Volcán de Colima (Mexico) and a block-and-ash flow from Mt. Meager (Canada) (Heap and Violay, 2021) were reduced when saturated with water. While wet to dry strength ratios in these lavas, which were relatively unaltered, were typically on the order of ~0.9, this ratio in tuffs can reach ~0.2 when the tuffs are characterised by high zeolite and clay mineral contents (Heap and Violay, 2021).

The importance of understanding the influence of water on the strength and mechanical behaviour of volcanic rocks is threefold. First, volcanoes are often saturated or partially-saturated and, in the case of subaerial, ocean-island, and coastal volcanoes, their saturation state also varies as a function of space and time (Hurwitz et al., 2003; Join et al., 2005; Aizawa et al., 2009; Delcamp et al., 2016). Volcanoes can be saturated, or partially-saturated, with meteoric water (approximately 45% of the world's active volcanoes lie in the Tropics and are therefore prone to intense periods of precipitation; Matthews et al., 2002), magmatic fluids, and, in the case of submarine, ocean-island, and coastal volcanoes, seawater. Second, modelling has shown that the mechanical properties of dome- and edifice-forming rock plays a first-order role in dictating their stability and therefore the risk of collapse and associated hazards (Apuani et al., 2005; Reid et al., 2001; Moon et al., 2009; Borselli et al., 2011; Schaefer et al., 2013; Heap et al., 2021a, 2021b; Harnett and Heap, 2021; Wallace et al., 2022; Mordensky et al., 2022; Harnett et al., 2022; Carr et al., 2022; Heap et al., 2023a) and so, if water-saturation reduces rock strength, it must also decrease dome and edifice stability. As a result, volcano stability models should, where and when appropriate, use the mechanical properties for water-saturated volcanic rocks. Third, the frequency of landslides and the failure and collapse of volcanic slopes and domes increases following heavy rainfall (Kerle and De Vries, 2001; Matthews et al., 2002; Matthews and Barclay, 2004; Elsworth et al., 2004; Simmons et al., 2004; Taron et al., 2007; Saucedo et al., 2008; Hicks et al., 2010; Vazquez et al., 2022), which will likely be exacerbated by the increase in heavy rainfall expected given the current trend in global warming (Farquharson and Amelung, 2022).

The paucity of laboratory data aimed at understanding water-weakening in volcanic rocks therefore hinders our ability to accurately assess the stability of volcanic domes and flanks. Further, not only does

hydrothermal alteration, a very common process at active volcanoes worldwide, influence the physical and mechanical properties of volcanic rocks (e.g., Frolova et al., 2014; Pola et al., 2014; Wyering et al., 2014; Mordensky et al., 2018; Coats et al., 2018; Heap et al., 2021a, 2021b; Darmawan et al., 2022; Kanakiya et al., 2021, 2022; Schaefer et al., 2023), but altered rocks can also contain the minerals (e.g., alunite and clay minerals) that are thought to promote water-weakening in volcanic rocks, and so it is of particular importance to assess the influence of hydrothermal alteration on water-weakening in volcanic rocks. Indeed, a deadly debris avalanche at Casita volcano (Nicaragua) in 1998 was thought to be the combined result of hydrothermal alteration and heavy rainfall (van Wyk de Vries et al., 2000; Kerle and De Vries, 2001; Kerle et al., 2003; Opfergelt et al., 2006), and a landslide on the northeastern side of the dome at Soufrière de Guadeloupe (Eastern Caribbean) that followed extreme rainfall exposed a collapse scar characterised by intensely hydrothermally altered materials (Fig. 1b).

Here, therefore, we present the results of (1) experiments designed to assess the influence of water-saturation on the mechanical properties of variably-altered volcanic rocks and (2) large-scale numerical modelling in Particle Flow Code (PFC), informed by the experimental data, that investigates the influence of water on the stability of a volcanic dome. For the purpose of this study, we will use La Soufrière de Guadeloupe as a case study.

## 2. Case study: La Soufrière de Guadeloupe (Eastern Caribbean)

La Soufrière de Guadeloupe is an active andesitic stratovolcano located on the French island of Guadeloupe in the Eastern Caribbean (Komorowski et al., 2005; Moretti et al., 2020; Fig. 1a). Volcanic unrest at La Soufrière de Guadeloupe has been steadily increasing in the last three decades, manifest as an increase in the number of acid chloride-sulfate springs and steam-dominated fumaroles, an increase in the heat output from the dome, an expansion of the outgassing area at the top of the dome, an increase in flank and summit displacement rates, and an abundance of shallow seismicity (including the largest felt tectonic earthquake since the last eruption in 1976–1977, and frequent earthquake swarms that include several hundreds of microearthquakes generated in few days and located within 1 km below the surface) (Brombach et al., 2000; Villemant et al., 2005; Tamburello et al., 2019; Moretti et al., 2020; Heap et al., 2021a; Jessop et al., 2021; Moune et al., 2022). Historically, partial edifice collapse has been common at La Soufrière de Guadeloupe: at least nine flank collapses have occurred in the last 9150 years (Boudon et al., 2008; Komorowski et al., 2005; Legendre, 2012; Peruzzetto et al., 2019), the most recent of which occurred in 1530 CE. Extensive hydrothermal alteration has been identified as having a key role in these events, based on the abundance of altered materials within the associated debris avalanche deposits (Komorowski et al., 2005; Le Friant et al., 2006; Salaün et al., 2011; Rosas-Carbajal et al., 2016; Peruzzetto et al., 2019; Heap et al., 2021a). The existence of hydrothermal fluid reservoirs (Brothelande et al., 2014; Rosas-Carbajal et al., 2016, 2017), perched aquifers (Lesparre et al., 2014), and the presence of listric-shaped, low-strength layers formed by the superposition of flank-collapse slip surfaces within and below the La Soufrière de Guadeloupe dome are anticipated to control the dynamics of future flank collapses and other mass-wasting phenomena (Rosas-Carbajal et al., 2016; Peruzzetto et al., 2019).

Meteoric fluid input is also significant at La Soufrière de Guadeloupe; for example, fumarole analysis by de Bremond d'Ars and Gibert (2022) highlights that meteoric input exerts an importance control on the otherwise seemingly stochastic dynamics of the shallow hydrothermal system. The volcano consistently receives over 5 m of rainfall annually at its summit (Dessert et al., 2015), with as much as 30% of meteoric input infiltrating into the groundwater (Rad et al., 2007). As a result, frequent smaller mass-wasting events at La Soufrière de Guadeloupe have been directly related to intense rainfall events (Lesparre et al., 2014), including landslides concurrent with the passage of storms and

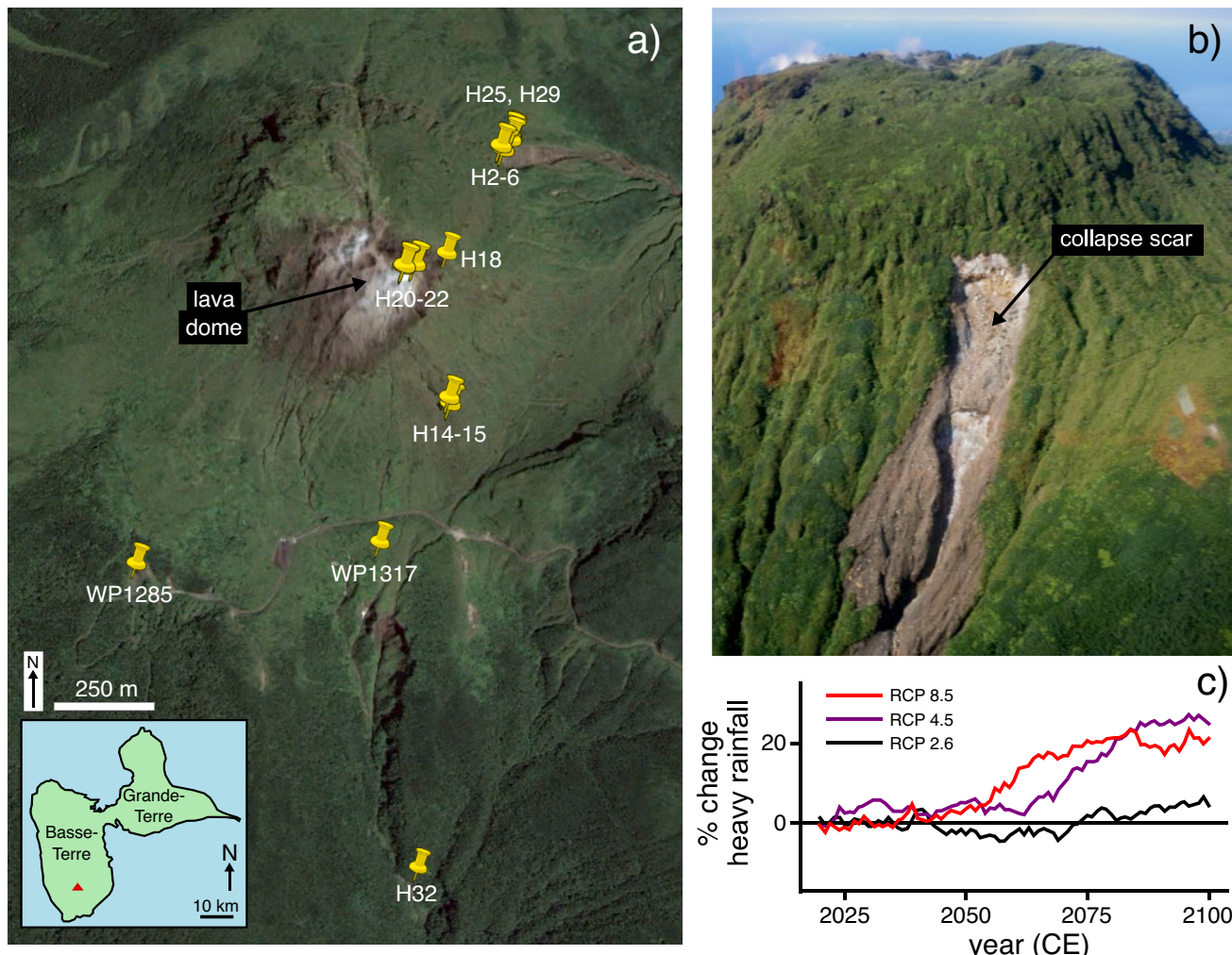


**Fig. 1.** (a) Google Earth image (Google Maxar Technologies CNES / Airbus) of La Soufrière de Guadeloupe showing the sampling locations for the 17 rock blocks collected for this study. Inset shows a map of Guadeloupe in which the location of La Soufrière de Guadeloupe is indicated by a red triangle. (b) Photograph of the 2009 landslide scar on the northeastern flank of the dome (taken on 12 December 2009; photo credit: J.-B. de Chabalier, IPGP-OVSG). (c) Percentage change in heavy rainfall predicted for La Soufrière de Guadeloupe. Data are from the MRI-CGCM3 General Circulation Model results, provided by the Meteorological Research Institute, Japan, via the Earth System Grid Federation servers (<https://esgf-node.llnl.gov/search/cmip5/>). The change in projected heavy rainfall is resampled from monthly results corresponding to the  $1.121 \times 1.125$  degree spatial grid containing La Soufrière de Guadeloupe, plotted as a function of time. For clarity, data are smoothed (15-year rolling mean) and normalised to 2023. Results are shown for three separate future climate scenarios: a high emissions scenario (RCP 8.6), an intermediate emissions scenario (RCP 4.5), and a “very stringent” pathway, whereby global carbon dioxide emissions decrease to zero within 80 years (RCP 2.6). Further details are given in Farquharson and Amelung (2022). (For interpretation of the references to colour in this figure legend, the reader is referred to the web version of this article.)

hurricanes (Allemand et al., 2014); one such example is shown in Fig. 1b. Very recently, parts of the *Chemin des Dames*, a tourist path on the west flank of the dome, required repair following small-volume, rain-induced landslides. This link between geohazards and the high-rainfall tropical climate echoes a broader trend of rainfall-induced hazards observed at volcanoes elsewhere in the Caribbean, including dome collapses (Matthews et al., 2002; Matthews and Barclay, 2004; Carn et al., 2004) and seismicity (Matthews et al., 2009). In a comparative analysis of global climate models, Farquharson and Amelung (2022) showed that models consistently project an increase in heavy rainfall across the volcanic areas of the Caribbean over the next eight decades. In Fig. 1c, we plot projected change in heavy rainfall over La Soufrière de Guadeloupe obtained from the MRI-CGCM3 general circulation model of Japan's Meteorological Research Institute: clearly, the propensity for heavy rainfall events is set to increase in the near future (see also Cane et al., 2014), even under the most ambitious climate change mitigation strategies (i.e. RCP 2.6).

Together, these factors highlight that La Soufrière de Guadeloupe

represents an ideal natural laboratory to study the influence of water-saturation on the physical and mechanical properties of volcanic rock and volcano stability.

### 3. Materials and methods

#### 3.1. Experimental materials

A suite of 17 variably altered andesite blocks from La Soufrière de Guadeloupe were used for this study (sampling locations are shown in Fig. 1a). Eight of the 17 blocks were collected from a collapse scar to the northeast of dome summit (blocks H2A, H2B, H3, H4A, H5A, H6, H25, and H29). Four blocks were collected from the dome summit: one block from the wall of the *Lacroix Supérieur* outgassing fracture on the lava dome (H18), and three blocks from the lava spines that protrude the top of the current dome (one block from *Cratère Sud Central*, H20, and two blocks from an adjacent site, H21 and H22). A block was collected to the southwest of dome summit from a collapse scar into a highly fractured

lava that forms the core of a paleo-collapse mega-block of the former volcanic edifice (WP1285). Blocks were also collected from the West wall of the fault “*Faillle du 30 août*” on the lava dome (H14 and H15), and from a thick lava adjacent to the Galion waterfall (H32). The final block is a volcanic non-juvenile bomb from the dome that was ejected during the 1976–1977 explosive eruption (Komorowski et al., 2005) and landed on the roof of a small disused thermal bathhouse to the south of the dome summit (WP1317). We climbed on the roof of the bathhouse to collect the block.

These 17 blocks, previously described by Heap et al. (2021a, 2022a, 2022b, 2022c, 2023a, 2023b), are porphyritic andesites characterised by a microcrystalline groundmass containing phenocrysts of dominantly plagioclase and pyroxene (orthopyroxene and clinopyroxene). The mineral assemblage present in each block was identified by a combination of optical microscopy, Raman spectroscopy, and X-ray powder diffraction (XRPD), and quantitative phase analysis was performed using the XRPD data and the Rietveld approach (for more details see Heap et al., 2021a). The XRPD data show that all of the rocks contain variable quantities of secondary (alteration) minerals: kaolinite, alunite or natro-alunite, silica polymorphs (quartz, cristobalite, tridymite, and opal-A), hematite, pyrite, gypsum, and talc (Heap et al., 2021a, 2022a, 2022b, 2022c; Table 1). In this contribution, we quantify alteration as the wt% of secondary minerals in each block. The predominant hydrous alteration phases are kaolinite, natro-alunite, and opal-A (Table 1), suggesting fluid-rock interaction with acidic sulfate-chloride-rich fluids at relatively low temperatures (<150–200 °C) (Inoue, 1995; Zimbelman et al., 2005; Scher et al., 2013; Fulignati, 2020; Heap et al., 2021a).

### 3.2. Experimental methods

Cylindrical samples were prepared from each of the blocks to a diameter of 20 mm and then cut and precision-ground to a nominal length of 40 mm. The cylindrical samples cored from a particular block were assumed to have the same mineral contents as the parent block (i.e. those listed in Table 1). The samples were first washed using tapwater and then dried in a vacuum-oven at 40 °C for at least 48 h. The connected porosity of all the samples was calculated using the bulk sample volume and the skeletal (solid) sample volume of the oven-dry samples measured by a helium pycnometer. Relative uncertainties of measurements of connected porosity are <2%.

Dry uniaxial compressive strength was measured on multiple oven-dry samples from all 17 blocks in a uniaxial load frame located in the laboratory at the Strasbourg Institute of Earth & Environment (ITES, France) (Fig. 2a). Samples were deformed under ambient laboratory pressure and temperature at a constant axial strain rate of  $10^{-5} \text{ s}^{-1}$  until macroscopic failure. Axial displacement and axial load were measured

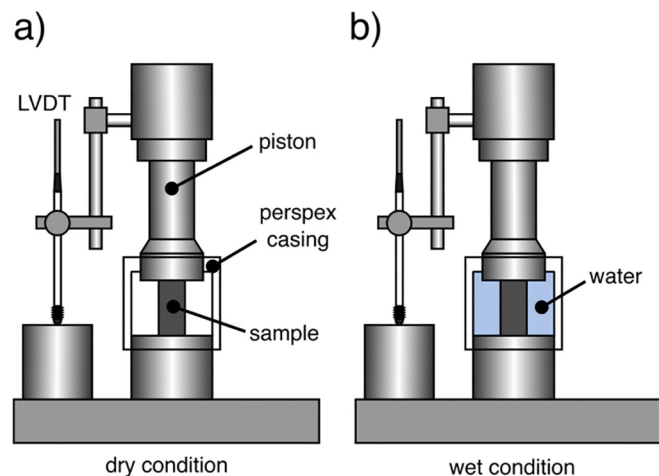


**Fig. 2.** Schematic diagrams of the uniaxial compression apparatus at the Strasbourg Institute of Earth & Environment (ITES). (a) Setup for the dry experiments. (b) Setup for the wet experiments.

using a linear variable differential transducer and a load cell, respectively. Axial displacement (minus the displacement accumulated within the load chain) and axial load were converted to axial strain and axial stress using the sample dimensions. Relative uncertainties of measurements of uniaxial compressive strength are <1%. The static Young's modulus was determined from the elastic portion of the uniaxial stress-strain curves (Heap et al., 2020a). Relative uncertainties of measurements of Young's modulus are <2%. The uniaxial compressive strength and Young's modulus of the samples deformed dry were previously published in Heap et al. (2021a) (with the exception of samples from block H32).

Water-saturated (wet) uniaxial compressive strength, data unique to this contribution, was measured on multiple samples from all 17 blocks using the same uniaxial load frame, inside a water bath (Fig. 2b). The samples to be deformed under saturated conditions were specifically selected so that their appearance and connected porosity was the same, or very similar, to the samples deformed under dry conditions from the same block (so that their dry and wet uniaxial compressive strength and Young's modulus can be compared directly). To do so, multiple samples were prepared from each block and only those with a similar appearance and porosity were selected for experimentation. Using this approach, the porosity difference between each sample pair was in the range 0.00–0.03, which we consider to be sufficient to allow for direct comparisons between the dry and wet uniaxial compressive strength and

**Table 1**

Mineral contents of the 17 rock blocks from La Soufrière de Guadeloupe measured by X-ray powder diffraction. Values in wt%. Asterisk denotes a secondary mineral (i.e. alteration mineral). Data from Heap et al. (2021a, 2022a, 2022b, 2022c). The relative uncertainties in the quantification are in the order of 5–10%. Sample locations are provided in Fig. 1a.

Mineral	H2A	H2B	H3	H4A	H5A	H6	H14	H15	H18	H20	H21	H22	H25	H29	H32	WP1285	WP1317
Plagioclase	56.7	12.3	46.6	23.3	41.3	30.0	60.7	22.5	61.2	28.7	24.2	59.5	38.7	62.4	64.4	64.7	61.6
Clinopyroxene	8.7	3.4	5.6	4.9	5.2	6.4	6.3	7.3	8.4	8.9	12.4	8.9	5.3	7.8	9.5	5.2	5.9
Orthopyroxene	10.8	9.5	11.8	11.8	11.1	10.8	8.6	9.2	12.2	15.0	19.3	13.6	10.2	11.2	15.1	13.2	15.6
(Ti-) Magnetite	0.7	–	0.8	–	–	–	0.8	–	2.9	2.4	3.1	0.8	–	2.7	4.9	3.5	0.7
Quartz*	1.0	0.5	0.6	0.6	0.5	0.5	1.7	0.7	0.7	0.3	0.2	0.6	0.3	0.4	0.3	0.2	0.7
Cristobalite*	11.3	12.8	10.6	11.8	13.0	11.1	13.5	10.2	11.7	11.4	11.7	10.6	9.8	12.4	5.7	–	–
Tridymite*	–	–	–	–	–	–	–	0.7	–	–	–	–	–	–	–	13.2	13.2
Hematite*	–	–	–	–	–	–	3.4	–	2.8	–	–	–	–	3.1	–	–	–
Pyrite*	3.5	–	3.8	2.3	–	–	–	–	–	–	0.4	3.1	0.6	–	–	–	–
Alunite*	–	–	–	–	–	–	–	–	–	–	–	–	–	–	–	–	2.4
Na-Alunite*	1.4	1.6	2.8	1.3	5.4	5.1	5.1	15.0	–	0.5	0.5	–	9.8	–	–	–	–
Gypsum*	–	–	–	0.7	–	–	–	–	–	0.8	1.2	–	–	–	–	–	–
Kaolinite*	6	59.7	17.4	43.3	23.5	36.0	< 1	34.3	–	2.0	2.0	< 1	25.3	–	–	–	–
Talc*	–	–	–	–	–	–	–	–	–	–	–	2.9	–	–	–	–	–
Opal-A*	–	–	–	–	–	–	–	–	–	30	25	–	–	–	–	–	–

Young's modulus of each of the blocks. Prior to deformation, the samples were vacuum-saturated in de-aired, deionised water. The water-saturation procedure was as follows. (1) The samples were placed inside a glass container, which was then placed within a bell jar. (2) The samples were vacuumed inside the bell jar for at least 12 h at room temperature. (3) Maintaining the vacuum inside the bell jar, de-aired, deionised water was introduced into the glass container until the samples were completely submerged. (4) The samples were left submerged within the vacuumed bell jar for at least 6 h, after which the vacuum was released and the glass container containing the samples was removed from the bell jar. (5) The samples remained submerged in de-aired, deionised water until deformed. As for the dry experiments, the static Young's modulus was then determined from the elastic portion of the uniaxial stress-strain curves. Samples from block H32, too strong to measure in the uniaxial load frame at the ITES, were measured at the Laboratory of Experimental Rock Mechanics at the Ecole Polytechnique Fédérale de Lausanne (EPFL, Switzerland) using a similar uniaxial setup. We consider the dry samples deformed in Heap et al. (2021a) to have a water saturation of 0%, and the wet samples deformed herein to have a water saturation of 100%.

Although rock strength and Young's modulus will increase as a function of pressure (or depth) in the brittle regime, we highlight that lava domes are typically only a few hundred metres high (the lava dome at La Soufrière de Guadeloupe, for example, is about 250–300 m high) and that rock physical and mechanical properties (e.g., uniaxial compressive strength and Young's modulus) will not change significantly under pressures representative of a depth of a few hundred metres.

### 3.3. Numerical modelling

To explore the effect of water-saturation on dome stability, we used 2D Discrete Element Method (DEM) models created in Particle Flow Code (PFC; Itasca Consulting Group Ltd), following the methods outlined by Harnett et al. (2018) and Harnett and Heap (2021). PFC has been previously used to successfully model the mechanical behaviour of rock (e.g., Potyondy and Cundall, 2004) and, recently, to model dome growth and collapse (Husain et al., 2014, 2018; Harnett et al., 2018; Husain et al., 2019; Harnett and Heap, 2021; Harnett et al., 2022; Walter et al., 2022; Heap et al., 2023a). These DEM models consider a particle-based material in which circular particles interact at interparticle contacts. Contact behaviour is primarily governed by stiffness and cohesion. At the boundary between the particles and walls (i.e. the ground surface), the contact behaviour is cohesionless and governed by friction. The particle size in the model is not representative of individual crystals, grains, or rock blocks, but rather represents discretisation of the medium for the purpose of computation.

First, we numerically generated two fully solid domes (see Harnett and Heap, 2021) containing 9745 circular particles and 22,710 contacts. The contact properties were guided by our experimental data for dry unaltered and altered dome rocks (uniaxial compressive strength, tensile strength, and Young's modulus). An iterative calibration procedure was required to relate contact parameters to bulk rock parameters, whereby uniaxial compression tests are reproduced in PFC (see Harnett and Heap (2021) for details). Using these calibrated parameters, we created initially stable dry unaltered and altered domes. These stable domes will not deform unless perturbed in some way. To explore the effect of water-saturation on the stability of these domes, we modified the mechanical properties of the contacts in the domes to represent wet unaltered and altered dome rocks, also guided by our experimental data. The model then provided the displacement within the dome resulting from water-saturation. Finally, we generated another initially stable fully solid dome using properties representative of dry unaltered rock. In a first scenario, we perturbed the dome by including a dry altered zone within the dome (as in Harnett et al., 2022). In a second scenario, we also included the buried altered zone within the dome, but, instead, we used

properties representative of wet unaltered and altered rock. We highlight that, although we use properties representative of uniaxial conditions in our models and, therefore, we do not explicitly consider an increase in strength with depth in the model, the models have an inherent depth-dependence of mechanical properties through the inclusion of gravity: the contact forces at the base of the dome are much higher than those at the surface of the dome. Further, as mentioned above, we also do not expect rock physical and mechanical properties (e.g., uniaxial compressive strength and Young's modulus) to change significantly under pressures representative of a depth of a few hundred metres. For the modelling of much larger, or deeper, features, we recommend that triaxial deformation experiments are performed to understand how rock physical and mechanical properties evolve as a function of pressure (depth).

## 4. Results

Representative uniaxial stress-strain curves for dry and wet samples are shown in Fig. 3 (for block H6). We highlight that the connected porosity of the dry and wet H6 samples shown in Fig. 3 is 0.18 and 0.16, respectively (Table 2). These curves show that the uniaxial compressive strength and the Young's modulus (the slope of the stress-strain curve in the pseudo-linear elastic regime) are lower when the sample is wet. We also note that the axial strain at the peak stress is slightly lower for the wet sample than for the dry sample (Fig. 3).

Dry (black circles) and wet (blue squares) uniaxial compressive strength data are plotted as a function of connected porosity and the wt % of secondary minerals in Fig. 4a and b, respectively (data available in Table 2). These data show that uniaxial compressive strength decreases as a function of connected porosity and the wt% of secondary minerals. For example, strength decreased from ~270 MPa to only a couple of MPa as porosity decreased from ~0.05 to >0.4 (Fig. 4a). These data also show that, for a given porosity, the strength of wet samples is typically lower than the strength of dry samples. Block H2B (porosity ~0.45; alteration 75 wt%; Table 2) and block H2A (porosity ~0.18; alteration 23 wt%) are characterised by the lowest and highest ratio of wet to dry strength, respectively.

We also show dry (black circles) and wet (blue squares) Young's modulus as a function of connected porosity and the wt% of secondary minerals in Fig. 4c and d, respectively (data available in Table 2). Similar to the strength data of Fig. 4a and b, the data of Fig. 4c and d show that (1) Young's modulus decreases as a function of connected

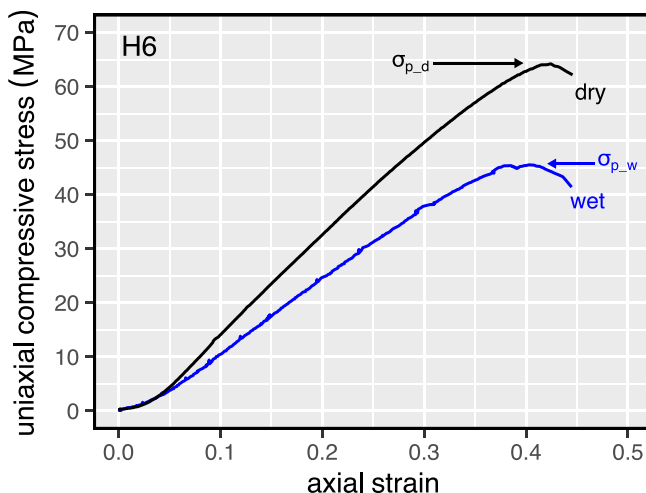


**Fig. 3.** Representative stress-strain curves for dry (black curve) and wet (blue curve) samples from block H6 from La Soufrière de Guadeloupe (Eastern Caribbean). The dry,  $\sigma_{p-d}$ , and wet,  $\sigma_{p-w}$ , uniaxial compressive strengths are indicated on the curves. (For interpretation of the references to colour in this figure legend, the reader is referred to the web version of this article.)

**Table 2**

Experimental condition (dry or wet), connected porosity, uniaxial compressive strength, Young's modulus, and the percentage of secondary minerals (i.e. alteration) for the samples prepared for this study. Sample locations are provided in Fig. 1a. Dry data (apart from data for H32) are from Heap et al. (2021a). The relative uncertainties of the connected porosity, uniaxial compressive strength, and Young's modulus are <2%, <1%, and <2%, respectively. The relative uncertainties in the quantification of the mineral contents (Table 1) are on the order of 5–10%.

Sample	Weight percentage of secondary minerals	Connected porosity	Condition	Uniaxial compressive strength (MPa)	Young's modulus (GPa)
H2A_2	23	0.18	Dry	63.7	31.9
H2A_5	23	0.19	Dry	80.5	25.5
H2A_6	23	0.19	Dry	65.4	25.8
H2A_11	23	0.19	Dry	59.3	24.4
H2A_12	23	0.18	Dry	70.4	28.0
H2A_7	23	0.17	Wet	66.3	26.4
H2A_10	23	0.16	Wet	59.9	22.3
H2A_14	23	0.20	Wet	40.7	17.7
H2B_3	75	0.42	Dry	6.6	1.8
H2B_10	75	0.42	Dry	6.4	1.9
H2B_11	75	0.41	Dry	8.7	2.3
H2B_12	75	0.41	Dry	8.1	2.3
H2B_15	75	0.43	Dry	4.6	1.6
H2B_7	75	0.44	Wet	2.0	0.2
H2B_9	75	0.47	Wet	2.0	0.7
H2B_13	75	0.44	Wet	2.4	0.8
H3_3	35	0.16	Dry	70.3	27.3
H3_7	35	0.16	Dry	69.9	24.9
H3_8	35	0.16	Dry	64.8	27.5
H3_11	35	0.16	Dry	59.7	24.0
H3_13	35	0.16	Dry	71.2	26.2
H3_14	35	0.17	Wet	31.5	9.8
H3_15	35	0.15	Wet	59.0	25.3
H4A_2	60	0.23	Dry	40.3	10.4
H4A_4	60	0.23	Dry	42.0	10.6
H4A_6	60	0.23	Dry	43.9	8.1
H4A_8	60	0.23	Dry	37.2	9.3
H4A_9	60	0.22	Dry	40.4	9.9
H4A_5	60	0.25	Wet	22.9	0.77
H4A_7	60	0.26	Wet	23.3	8.3
H4A_10	60	0.24	Wet	22.0	7.8
H5A_2	42	0.16	Dry	88.3	26.4
H5A_3	42	0.16	Dry	86.6	22.8
H5A_5	42	0.16	Dry	83.9	22.5
H5A_8	42	0.18	Dry	68.8	21.2
H5A_10	42	0.17	Dry	74.5	23.0
H5A_4	42	0.20	Wet	48.8	18.4
H5A_9	42	0.15	Wet	64.5	23.4
H6_6	53	0.18	Dry	55.1	13.5
H6_9	53	0.18	Dry	68.0	18.0
H6_9	53	0.18	Dry	53.0	12.5
H6_12	53	0.18	Dry	64.2	17.6
H6_13	53	0.18	Dry	63.0	18.3
H6_2	53	0.16	Wet	45.5	13.5
H6_3	53	0.20	Wet	39.2	11.8
H6_5	53	0.17	Wet	40.7	12.6
H14_2	24	0.18	Dry	65.4	26.1
H14_3	24	0.21	Dry	21.1	11.6
H14_5	24	0.21	Dry	26.8	13.1
H14_6	24	0.19	Dry	29.8	12.1
H14_10	24	0.21	Dry	16.1	6.6
H14_8	24	0.20	Wet	12.5	9.7
H14_11	24	0.18	Wet	40.7	11.0
H15_3	61	0.28	Dry	24.6	10.0
H15_4	61	0.28	Dry	27.1	11.0
H15_5	61	0.29	Dry	22.8	9.4
H15_6	61	0.27	Wet	17.3	9.5
H15_7	61	0.25	Wet	12.7	8.7
H18_3	15	0.13	Dry	101.3	37.9
H18_4	15	0.13	Dry	89.8	39.1
H18_5	15	0.13	Dry	98.8	41.0
H18_6	15	0.13	Dry	93.2	43.1
H18_7	15	0.13	Dry	113.7	35.1
H18_11	15	0.13	Wet	65.7	20.3
H18_14	15	0.12	Wet	94.7	35.3
H20_2	45	0.37	Dry	4.8	1.2
H20_3	45	0.37	Dry	4.4	1.3
H20_7	45	0.37	Dry	4.6	1.4
H20_8	45	0.37	Dry	6.1	1.8
H20_10	45	0.37	Dry	3.4	1.1
H20_5	45	0.39	Wet	3.9	0.9

(continued on next page)

**Table 2** (continued)

Sample	Weight percentage of secondary minerals	Connected porosity	Condition	Uniaxial compressive strength (MPa)	Young's modulus (GPa)
H20_6	45	0.40	Wet	3.1	0.7
H20_11	45	0.36	Wet	3.1	1.1
H21_3	41	0.17	Dry	90.2	26.6
H21_8	41	0.16	Dry	65.2	17.4
H21_11	41	0.16	Dry	86.9	25.8
H21_12	41	0.16	Dry	73.8	19.2
H21_13	41	0.16	Dry	87.2	20.1
H21_4	41	0.17	Wet	71.3	19.5
H21_6	41	0.18	Wet	44.1	12.8
H21_15	41	0.17	Wet	55.8	18.1
H22_2	17	0.12	Dry	145.7	29.7
H22_3	17	0.12	Dry	144.3	30.1
H22_4	17	0.12	Dry	139.1	30.5
H22_5	17	0.12	Dry	149.7	28.9
H22_6	17	0.12	Dry	133.6	31.1
H22_7	17	0.12	Wet	119.6	26.2
H22_14	17	0.12	Wet	131.3	24.8
H22_15	17	0.13	Wet	113.6	21.5
H25_2	46	0.14	Dry	99.9	29.3
H25_4	46	0.14	Dry	97.7	29.3
H25_5	46	0.14	Dry	94.2	26.2
H25_9	46	0.14	Dry	87.1	29.9
H25_12	46	0.15	Dry	83.1	24.0
H25_3	46	0.18	Wet	38.2	19.2
H25_10	46	0.13	Wet	72.9	24.2
H25_14	46	0.14	Wet	75.0	24.9
H29_2	16	0.22	Dry	53.9	25.4
H29_8	16	0.23	Dry	59.1	24.5
H29_9	16	0.22	Dry	75.2	27.9
H29_12	16	0.25	Dry	53.4	23.5
H29_16	16	0.24	Dry	50.7	21.3
H29_3	16	0.20	Wet	59.4	21.2
H29_6	16	0.26	Wet	34.8	24.2
H29_13	16	0.23	Wet	29.5	24.9
H32_1	6	0.04	Dry	270.1	–
H32_4	6	0.05	Dry	263.9	–
H32_5	6	0.05	Dry	271.9	–
H32_6	6	0.04	Dry	274.5	–
H32_7	6	0.04	Dry	252.6	–
H32_8	6	0.05	Wet	194.1	–
H32_9	6	0.05	Wet	204.6	–
H32_10	6	0.04	Wet	212.2	–
WP1285_2	13	0.13	Dry	78.5	22.8
WP1285_8	13	0.13	Dry	63.0	25.7
WP1285_10	13	0.13	Dry	78.3	21.4
WP1285_11	13	0.12	Dry	87.2	21.1
WP1285_15	13	0.12	Dry	84.6	25.6
WP1285_4	13	0.12	Wet	66.1	17.7
WP1285_6	13	0.12	Wet	57.3	18.8
WP1285_9	13	0.12	Wet	66.8	22.5
WP1317_2	16	0.16	Dry	67.3	20.4
WP1317_6	16	0.16	Dry	84.5	24.7
WP1317_7	16	0.15	Dry	91.5	22.6
WP1317_8	16	0.15	Dry	95.8	25.9
WP1317_12	16	0.15	Dry	104.0	24.7
WP1317_10	16	0.15	Wet	74.8	25.5
WP1317_13	16	0.14	Wet	89.6	26.2
WP1317_15	16	0.14	Wet	95.9	25.5

porosity and the wt% of secondary minerals and (2) for a given porosity, the Young's modulus of wet samples is typically lower than the Young's modulus of dry samples. For example, Young's modulus decreased from ~40 GPa to only a couple of GPa as porosity increases from ~0.05 to >0.4 (Fig. 4c) or as the wt% of secondary minerals increases from ~15 to ~75 wt% (Fig. 4d). Block H2B (porosity ~0.45; alteration 75 wt%; Table 2) and block WP1317 (porosity ~0.14; alteration 16 wt%) are characterised by the lowest and highest ratio of wet to dry Young's modulus, respectively.

To better highlight the difference between wet and dry strength and Young's modulus, the ratio of wet to dry strength and the ratio of wet to dry Young's modulus are plotted as a function of connected porosity and the wt% of secondary minerals in Fig. 5 (data available in Table 3). This ratio is obtained by organising the samples from the same block

deformed under dry and wet conditions into pairs, and then dividing the data for the sample deformed under saturated conditions with the data for their corresponding dry counterpart. As mentioned above, the samples deformed under saturated conditions were specifically selected so that their appearance and porosities were the same, or very similar, to those deformed under dry conditions. A ratio of one therefore corresponds to the scenario in which the dry and wet properties are exactly the same, and a ratio below and above one indicates that the sample property is lower or higher when wet, respectively. Fig. 5a shows that all of the samples have a wet to dry strength lower than one, indicating that all samples were weaker when saturated with water. These data also show that the wet to dry strength ratio appears to decrease as a function of increasing porosity (Fig. 5a) and wt% of secondary minerals (Fig. 5b). Fig. 5c shows that the majority of the samples have a wet to dry Young's

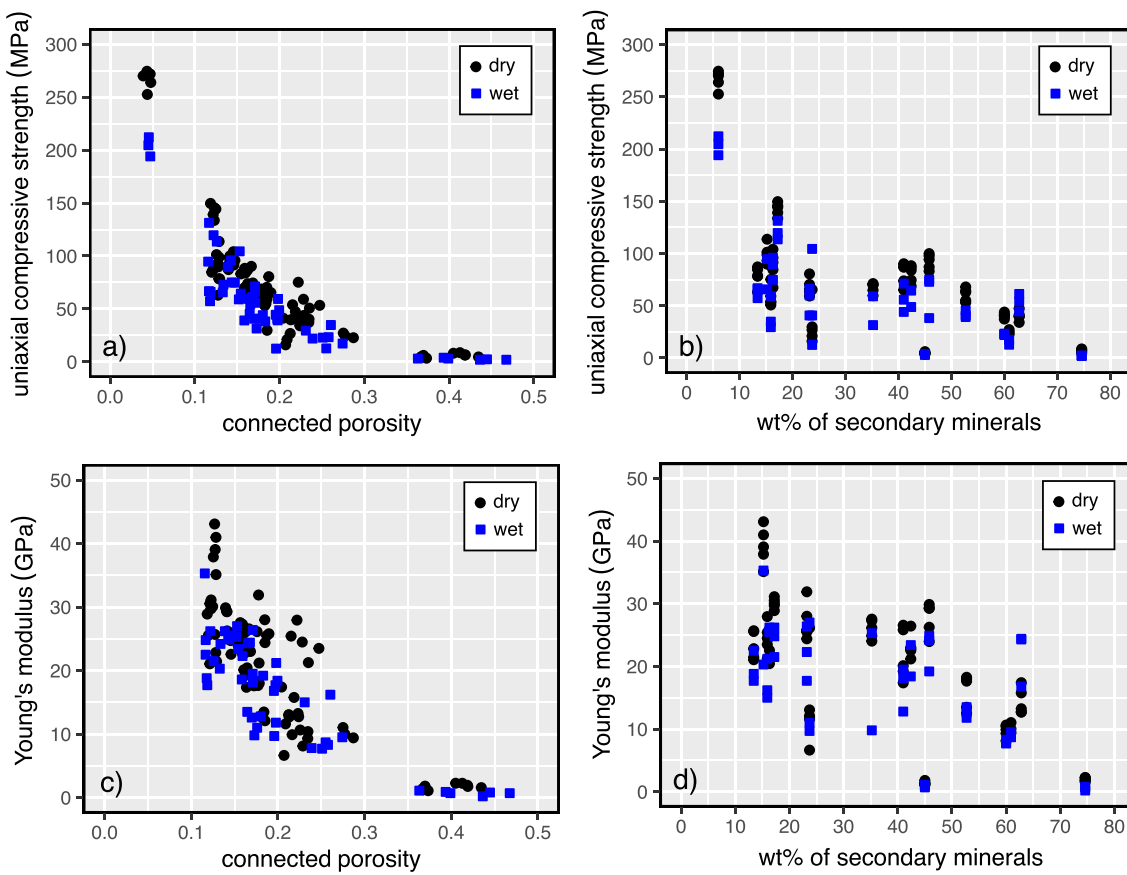


**Fig. 4.** Uniaxial compressive strength of dry (black circles) and wet (blue squares) samples from La Soufrière de Guadeloupe (Eastern Caribbean) as a function of (a) connected porosity and (b) the wt% of secondary minerals. Young's modulus of dry and wet samples from La Soufrière de Guadeloupe as a function of (c) connected porosity and (d) the wt% of secondary minerals. Dry data (apart from data for H32) are from Heap et al. (2021a). The relative uncertainties of the connected porosity, uniaxial compressive strength, and Young's modulus are <2%, < 1%, and < 2%, respectively; the uncertainties are therefore captured by the symbol size. The relative uncertainties in the quantification of the mineral contents (Table 1) are on the order of 5–10%. (For interpretation of the references to colour in this figure legend, the reader is referred to the web version of this article.)

modulus ratio below one. Although the wet to dry Young's modulus ratio appears to decrease as a function of increasing porosity (Fig. 5c), there appears to be no discernible trend as a function of increasing wt% of secondary minerals (Fig. 5d), although we highlight that the samples with the lowest wet to dry Young's modulus ratio contain the highest proportion of secondary minerals (Fig. 5d).

## 5. Discussion

### 5.1. Water-weakening in volcanic rocks: The influence of porosity

Our data show that the uniaxial compressive strength and Young's modulus of variably-altered dome lavas from La Soufrière de Guadeloupe are reduced when water-saturated (Figs. 4 and 5), in agreement with previous studies on volcanic rocks (Zhu et al., 2011; Heap et al., 2015; Zhu et al., 2016; Heap et al., 2018; Kendrick et al., 2021; Heap and Violay, 2021).

We plot the ratio of wet to dry strength and the ratio of wet to dry Young's modulus as a function of connected porosity for our new data alongside published data for volcanic rocks in Fig. 6a and b, respectively. Fig. 6a and b show that, based on previously published data for andesite, basalt, dacite, and welded block-and-ash flow, one would conclude that water-weakening in volcanic rocks does not appear to vary systematically with porosity. Previous studies have also shown that porosity does not appear to influence water-weakening in sandstones (Heap et al., 2019), limestones (Baud et al., 2016), and tuffs (Zhu et al., 2011; Heap et al., 2018; Frolova et al., 2021). Our new data for

hydrothermally altered andesites from La Soufrière de Guadeloupe, however, suggest that porosity exerts influence on their water-weakening behaviour (Fig. 6a and b). This may be because the porosity range studied in previous contributions was insufficient to observe a trend (the most porous sample from the previously published dataset is a dacite with a porosity of ~0.3, whereas the maximum porosity in our dataset is ~0.45; Fig. 6 and b). Although we conclude that porosity appears to exert influence on water-weakening in our sample suite, we suggest that more data for high-porosity volcanic rocks are now required to make firm conclusions as to the influence of porosity on water-weakening in volcanic rocks (based on reasoning discussed in the next subsection).

### 5.2. Water-weakening in volcanic rocks: The influence of alteration

We first note that the uniaxial compressive strength (Fig. 4b) and Young's modulus (Fig. 4d) of water-saturated andesites from La Soufrière de Guadeloupe are reduced as a function of increasing wt% of secondary minerals. Previously, hydrothermal alteration has been shown to either decrease (e.g., Frolova et al., 2014; Pola et al., 2014; Wyering et al., 2014; Mordensky et al., 2018, 2019; Heap et al., 2021a; Darmawan et al., 2022; Schaefer et al., 2023) or increase the strength of volcanic rocks (e.g., Frolova et al., 2014; Pola et al., 2014; Wyering et al., 2014; Coats et al., 2018; Heap et al., 2020b, 2021b). These studies, and others, have shown that whether or not hydrothermal alteration decreases or increases strength depends on the type of alteration and/or whether the alteration results in increases or decreases in porosity.

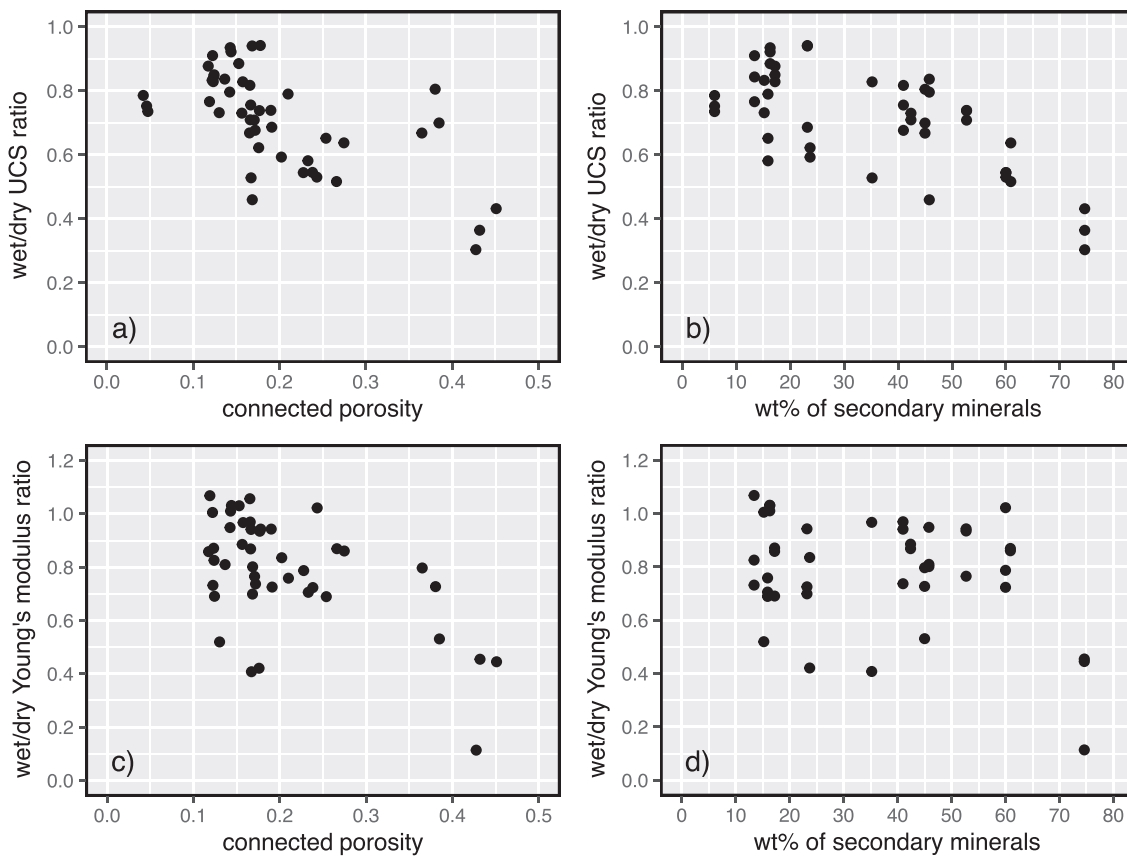


**Fig. 5.** Ratio of wet to dry uniaxial compressive strength (UCS) for samples from La Soufrière de Guadeloupe (Eastern Caribbean) as a function of (a) connected porosity and (b) the wt% of secondary minerals. Ratio of wet to dry Young's modulus for samples from La Soufrière de Guadeloupe as a function of (c) connected porosity and (d) the wt% of secondary minerals. The relative uncertainties of the connected porosity, uniaxial compressive strength, and Young's modulus are <2%, < 1%, and < 2%, respectively; the uncertainties are therefore captured by the symbol size. The relative uncertainties in the quantification of the mineral contents (Table 1) are on the order of 5–10%.

In the case of hydrothermally altered dome rocks from La Soufrière de Guadeloupe, Heap et al. (2021a, 2022a, 2022b, 2022c) concluded that alteration had reduced their uniaxial compressive strength and Young's modulus. However, these authors also noted that there is a relationship between porosity and alteration (Fig. 7). As discussed by these authors, it is difficult to unravel the influence of porosity and alteration on the strength of these materials because it is unclear whether alteration increased the porosity of the samples or whether the more porous samples are more altered due to their higher fluid-rock ratios. However, based on the presence of abundant clays and dissolution textures in these samples, Heap et al. (2021a, 2022a, 2022b, 2022c) concluded uniaxial compressive strength and Young's modulus were likely reduced by hydrothermal alteration. We conclude the same here, although we highlight that the main focus of this contribution is to study the influence of water-saturation on the mechanical properties of hydrothermally altered dome rocks, discussed below.

Our data suggest that the wet to dry strength ratio decreases as a function of increasing wt% of secondary minerals (Fig. 5b), although there appears to be no discernible trend in the wet to dry Young's modulus ratio as a function of increasing wt% of secondary minerals (Fig. 5d). In other words, these data suggest that the reduction in strength due to the presence of water increases as a function of the degree of hydrothermal alteration and, therefore, the abundance of secondary (alteration) minerals. These results are in agreement with the previous laboratory data for tuff, which suggest that the presence of alunite (Heap et al., 2015) and zeolites and clay minerals (Heap et al., 2018) may be responsible for the reduction in uniaxial compressive strength in the presence of water. Expansive clay minerals, for example, can mechanically degrade as a function of increasing water content

(Nara et al., 2012). The fact that alteration increases the observed water-weakening (Fig. 5b) and that alteration increases as a function of connected porosity for these rocks (Fig. 7) also suggests that the observed trends as a function of porosity (Fig. 6a and b) could be because the high-porosity rocks are more altered, and it is the alteration that is dictating the observed water-weakening. As stated above, more experiments are now required to make firm conclusions as to the influence of porosity on water-weakening in volcanic rocks.

To further investigate the influence of alteration on water-weakening, we replot the ratio of wet to dry uniaxial compressive strength and Young's modulus as a function of a subset of the alteration minerals (alunite, Na-alunite, gypsum, kaolinite, and talc only; i.e. excluding cristobalite, tridymite, hematite, pyrite, and opal-A) in Fig. 8. We include those minerals that have previously been considered to reduce the strength of rock upon water-saturation. We highlight that the coefficients of determination for simple linear fits to the data shown in Fig. 8 are very similar to those for the data shown in Fig. 5b and d. Therefore, these data suggest that the selected alteration minerals (alunite, Na-alunite, gypsum, kaolinite, and talc) are likely those influencing the uniaxial compressive strength of these rocks in the presence of water (Fig. 8a).

To investigate the mechanism responsible for the observed weakening in the presence of water, and the increase in water-weakening as a function of alteration (Figs. 4b, 5b, and 8a), we use the analytical approximation of Sammis and Ashby (1986) pore-emanating crack micromechanical model provided by Zhu et al. (2010):

$$UCS = \frac{1.325}{\phi^{0.414}} \frac{K_{IC}}{\sqrt{\pi r}} \quad (1)$$

**Table 3**

Percentage of secondary minerals (i.e. alteration), average connected porosity, the ratio of wet to dry uniaxial compressive strength, and the ratio of wet to dry Young's modulus for the samples prepared for this study. Sample locations are provided in Fig. 1a. The relative uncertainties of the connected porosity, uniaxial compressive strength, and Young's modulus are <2%, <1%, and <2%, respectively. The relative uncertainties in the quantification of the mineral contents (Table 1) are on the order of 5–10%.

Sample	Weight percentage of secondary minerals	Connected porosity	wet/dry UCS ratio	wet/dry Young's modulus ratio
H2A	23	0.17	0.94	0.70
H2A	23	0.18	0.94	0.94
H2A	23	0.19	0.69	0.73
H2B	75	0.45	0.43	0.45
H2B	75	0.43	0.30	0.11
H2B	75	0.43	0.36	0.45
H3	35	0.17	0.53	0.41
H3	35	0.16	0.83	0.97
H4A	60	0.23	0.54	0.79
H4A	60	0.24	0.55	0.72
H4A	60	0.24	0.53	1.02
H5A	42	0.16	0.73	0.89
H5A	42	0.17	0.71	0.87
H6	53	0.17	0.71	0.77
H6	53	0.19	0.74	0.94
H6	53	0.18	0.74	0.93
H14	24	0.20	0.59	0.84
H14	24	0.18	0.62	0.42
H15	61	0.27	0.64	0.86
H15	61	0.27	0.52	0.87
H18	15	0.12	0.83	1.01
H18	15	0.13	0.73	0.52
H20	45	0.38	0.81	0.73
H20	45	0.38	0.70	0.53
H20	45	0.36	0.67	0.80
H21	41	0.17	0.82	0.97
H21	41	0.17	0.68	0.74
H21	41	0.17	0.76	0.94
H22	17	0.12	0.85	0.69
H22	17	0.12	0.88	0.86
H22	17	0.12	0.83	0.87
H25	46	0.14	0.80	0.95
H25	46	0.14	0.84	0.81
H25	46	0.17	0.46	0.80
H29	16	0.21	0.79	0.76
H29	16	0.25	0.65	0.69
H29	16	0.23	0.58	0.71
H32	6	0.05	0.74	–
H32	6	0.05	0.75	–
H32	6	0.04	0.79	–
WP1285	13	0.12	0.77	1.07
WP1285	13	0.12	0.91	0.73
WP1285	13	0.12	0.84	0.83
WP1317	16	0.14	0.92	1.03
WP1317	16	0.14	0.93	1.01
WP1317	16	0.15	0.89	1.03

The pore-emanating crack model of Sammis and Ashby (1986) has been widely used to investigate the mechanical behaviour of porous volcanic rocks (see Heap and Violay (2021) for a review). The pore-crack model describes a two-dimensional elastic medium populated with circular pores of a uniform radius. In the model, cracks can propagate in a direction parallel to the maximum principal stress when the stress at the tip of a crack on the curved surface of the pore reaches the fracture toughness of the material,  $K_{IC}$  (the resistance of a brittle material to the propagation of cracks under an applied stress). Eventually, the cracks grow long enough to interact and ultimately coalesce, resulting in the macroscopic failure of the medium. Although the andesites studied here contain microcracks, their microstructure can be well approximated by this inclusion model (i.e. pores within a groundmass; Heap et al., 2021a), although we highlight that the model assumes a uniform pore radius. In the analytical solution to the model (Eq. (1)), uniaxial compressive strength (UCS) is a function of  $K_{IC}$ , porosity,  $\phi$ , and pore radius,  $r$ . The two unknowns in Eq. (1) are  $K_{IC}$  and  $r$ . We can estimate  $r$  using microstructural analysis. To do so, we calculated the average equivalent macropore diameter (excluding pores with a diameter < 30  $\mu\text{m}$ ) of each block using scanning electron microscope images and open-

source image analysis software ImageJ (data available in Table 4). The average equivalent macropore diameter,  $2r$ , was calculated using  $2r = 3/2(d_F)$ , where  $d_F$  is the average macropore Feret diameter. An example of how the average equivalent macropore diameter was determined is available as Supplementary Information. Values of dry and wet  $K_{IC}$  were then estimated using Eq. (1), taking the average values of dry and wet UCS for each block (Table 2). Dry and wet  $K_{IC}$ , and the wet to dry  $K_{IC}$  ratio, are plotted as a function of alteration in Fig. 9a and b, respectively (data available in Table 4). The data of Fig. 9 highlight that (1) wet  $K_{IC}$  is lower than dry  $K_{IC}$  and (2) the reduction in  $K_{IC}$  in the presence of water is increased as a function of increasing alteration. Using this approach, the wet to dry  $K_{IC}$  ratio for the andesites studied herein is estimated to be between 0.32 and 0.93 (Fig. 9). For the most part, these values are lower than those typically reported in published studies. For example, ratios for a suite of sandstones were measured to be between 0.65 and 0.95 (Noël et al., 2021), and the ratio for an unaltered andesite (Kumamoto andesite) was measured to be 0.87 (Nara et al., 2012). We emphasise that the values of  $K_{IC}$  provided in Fig. 9 and Table 4 are estimates made using the pore-emanating crack model (Eq. (1)), and not measured values of  $K_{IC}$  as in Noël et al. (2021) and Nara et al. (2012).

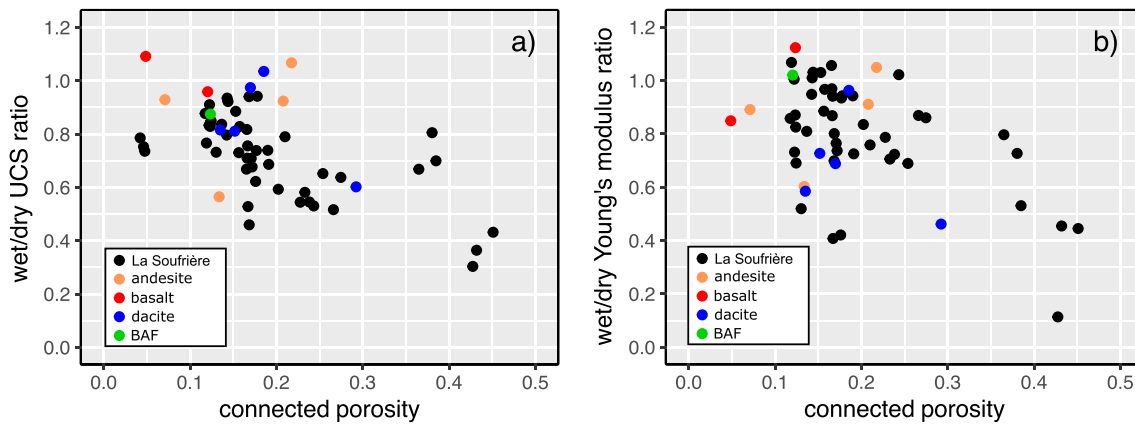


**Fig. 6.** Ratio of wet to dry (a) uniaxial compressive strength and (b) Young's modulus for samples from La Soufrière de Guadeloupe (Eastern Caribbean) as a function of connected porosity (black circles). Data for andesite (orange circles), basalt (red circles), and block-and-ash flow (BAF; green circles) from Heap and Violay (2021). Data for dacite (blue circles) from Kendrick et al. (2021). For the data for the samples from La Soufrière de Guadeloupe, the relative uncertainties of the connected porosity, uniaxial compressive strength, and Young's modulus are <2%, <1%, and <2%, respectively; the uncertainties are therefore captured by the symbol size. (For interpretation of the references to colour in this figure legend, the reader is referred to the web version of this article.)

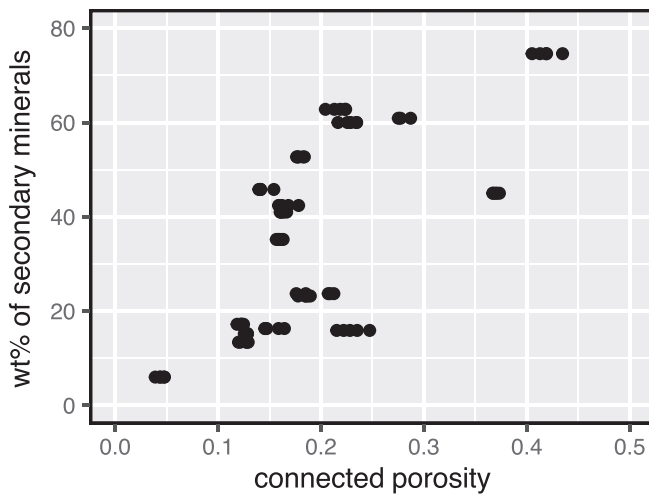


**Fig. 7.** The wt% of secondary minerals as a function of connected porosity for samples from La Soufrière de Guadeloupe (Eastern Caribbean).

A reduction in the  $K_{IC}$  of rocks in the presence of water has been observed by many experimental studies and has been attributed to several, potentially coeval, factors: a reduction in surface energy due to water adsorption (Baud et al., 2000; Noël et al., 2021), crack-tip capillary forces (Nara et al., 2012), grain-contact lubrication (Guha Roy et al., 2017), stress corrosion cracking (Kataoka et al., 2015), mineral dissolution (Maruvanchery and Kim, 2019), and the presence of clay minerals (Wang et al., 2007; Nara et al., 2012). The reduction in  $K_{IC}$  in the presence of water observed here (Fig. 9a), is likely due to a combination of these mechanisms; although, given that we provide here the short-term mechanical strength (UCS experiments performed at a strain rate of  $10^{-5} \text{ s}^{-1}$ ), we anticipate only minor contributions from stress corrosion cracking and mineral dissolution. We consider that the increase in the reduction in  $K_{IC}$  in the presence of water as alteration increases (Fig. 9b) is most likely explained by the increasing abundance of hydrophilic minerals, such as alunite and clay minerals, as a function of increasing alteration (Table 1). Hydrophilic minerals expand upon saturation with water, resulting in a reduction in their mechanical resistance (Nara et al., 2012). We further note that, if hydrophilic minerals expand upon saturation and reduce  $\phi$  and/or  $r$ , then the  $K_{IC}$  estimated for the altered rocks using Eq. (1) would be even lower than our estimations presented in Table 4 and Fig. 9.

We conclude, therefore, that the water-weakening in the dome rocks measured herein (i.e. the reduction in UCS; Figs. 4, 5, 6, and 8) is likely due to a reduction in  $K_{IC}$  in the presence of water (Fig. 9a). The increase in water-weakening as a function of alteration (Fig. 5b) can be explained by the decrease in the wet to dry  $K_{IC}$  ratio as the degree of alteration (i.e. the abundance of hydrophilic minerals) increases (Fig. 9b). The higher the wt% of secondary minerals such as alunite and clay minerals, the more  $K_{IC}$  is reduced when the rock is wet, and the greater the macroscopic water-weakening.

We highlight that we have performed experiments on completely dry and completely water-saturated samples. However, in nature, the rocks forming a volcanic edifice or dome likely exist between these two end-members (i.e. partially-saturated). Previous experimental work has shown that the water-weakening observed at 100% saturation in sandstones can be observed at saturation levels as low as 10%, whereas the compressive strength of shale decreased almost linearly as a function of increasing saturation level (Schmitt et al., 1994). Systematic uniaxial compressive strength measurements on partially-saturated volcanic rocks, which preserve different porosities and alteration intensities, are now required to understand whether the water-weakening observed here at 100% saturation (Fig. 5) is also observed at lower levels of saturation. Finally, we note that we have used deaired, deionised water for our experiments. However, hydrothermal fluids, for example, are often characterised by low values of pH (e.g., Delmelle et al., 2000) which can influence the short-term strength of rock (e.g., Singh et al., 1999). Future experimental studies should also explore the influence of fluid composition and pH on the short-term strength of variably porous and variably altered volcanic rock.

### 5.3. The influence of water-saturation on dome stability

We performed numerical simulations in PFC to better understand the influence of water-saturation on dome stability. As explained in our methods section above, we first prepared initially stable dry unaltered and altered domes, guided by our experimental data (Table 2). For the dry unaltered dome, we determined the contact bond parameters required to give uniaxial compressive strength, tensile strength, and Young's modulus values of 100 MPa, 10 MPa, and 25 GPa, respectively (Fig. 10a). These values were chosen to represent the samples in our dataset that are characterised by low levels of alteration (e.g., samples H18, H22, WP1317). For the dry altered dome, we determined the contact bond parameters required to give uniaxial compressive strength, tensile strength, and Young's modulus values of 10 MPa, 1 MPa, and 2 GPa, respectively (Fig. 10c). These values were chosen to represent the

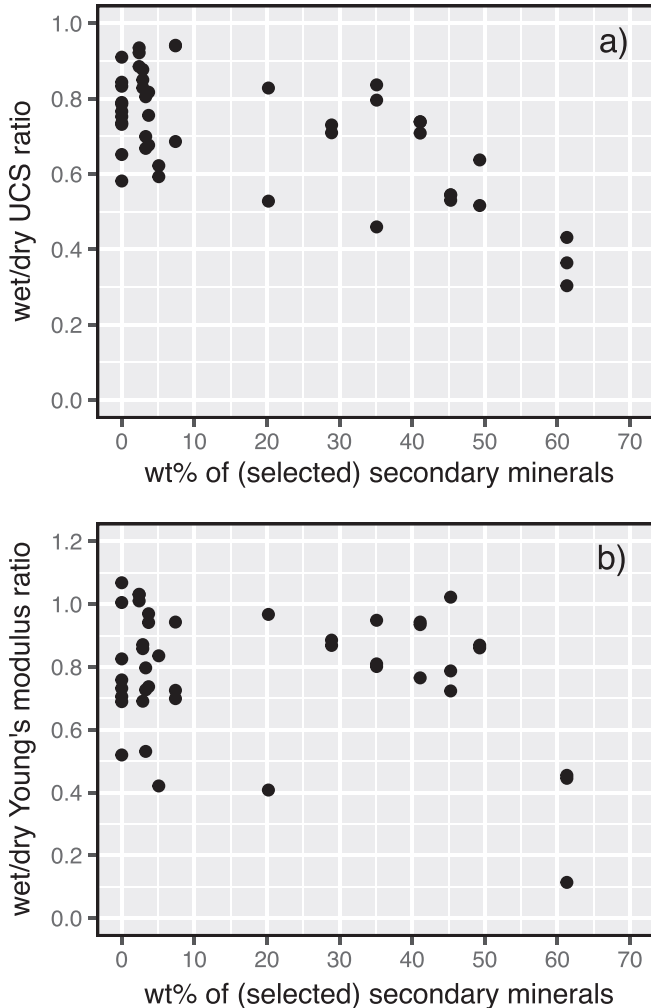


**Fig. 8.** Ratio of wet to dry (a) uniaxial compressive strength and (b) Young's modulus as a function of the wt% of a subset of the secondary minerals for samples from La Soufrière de Guadeloupe (Eastern Caribbean). The alteration minerals included are alunite, Na-alunite, gypsum, kaolinite, and talc only (i.e. excluding cristobalite, tridymite, hematite, pyrite, and opal-A). The relative uncertainties of the uniaxial compressive strength and Young's modulus are <1% and < 2%, respectively; the uncertainties are therefore captured by the symbol size. The relative uncertainties in the quantification of the mineral contents (Table 1) are on the order of 5–10%.

**Table 4**

Percentage of secondary minerals (i.e. alteration), average equivalent macropore diameter, wet fracture toughness ( $K_{IC}$ ), dry  $K_{IC}$ , and the wet to dry  $K_{IC}$  ratio for the samples prepared for this study. Sample locations are provided in Fig. 1b. Values of  $K_{IC}$  are estimated using the analytical approximation of Sammis and Ashby (1986) pore-emanating crack micromechanical model provided by Zhu et al. (2010) (Eq. (1)). The relative uncertainties in the quantification of the mineral contents (Table 1) are on the order of 5–10%.

Sample	Weight percentage of secondary minerals	Average equivalent macropore diameter, $r$ ( $\mu\text{m}$ )	Dry $K_{IC}$ ( $\text{MPa}\cdot\text{m}^{-1/2}$ )	Wet $K_{IC}$ ( $\text{MPa}\cdot\text{m}^{-1/2}$ )	Wet/dry $K_{IC}$ ratio
H2A	23	179	0.43	0.35	0.82
H2B	75	173	0.06	0.02	0.31
H3	35	174	0.39	0.26	0.68
H4A	60	153	0.26	0.15	0.57
H5A	42	161	0.45	0.32	0.71
H6	53	145	0.34	0.24	0.70
H14	24	156	0.26	0.16	0.62
H15	61	180	0.19	0.11	0.60
H18	15	137	0.47	0.38	0.81
H20	45	167	0.04	0.03	0.74
H21	41	157	0.45	0.32	0.71
H22	17	88	0.53	0.46	0.88
H25	46	182	0.52	0.31	0.60
H29	16	204	0.43	0.35	0.81
H32	6	101	0.73	0.46	0.63
WP1285	13	69	0.26	0.21	0.79
WP1317	16	84	0.35	0.32	0.93

samples in our dataset that are characterised by high levels of alteration (e.g., sample H2B). We used a bulk density of 2400 and 1500  $\text{kg}/\text{m}^3$  for unaltered and altered dry rocks, respectively, as guided by our experimental data. To investigate the influence of water-saturation at the dome scale, we then changed all of the contact bond parameters in the model to those representative of wet rocks (i.e. a completely water-saturated dome). Guided by our experimental data (Fig. 5b and d), we assumed wet to dry uniaxial compressive strength and Young's modulus ratios for unaltered and altered dome rocks of 0.9 and 0.4, respectively. Therefore, we determined the contact bond parameters required to give uniaxial compressive strength, tensile strength, and Young's modulus of 90 MPa, 9 MPa, and 20 GPa, respectively, for the unaltered dome (Fig. 10b) and, for the altered dome, we used values of 4 MPa, 0.4 MPa, and 1 GPa, respectively (Fig. 10d). We also note that, similar to the experimental data shown in Fig. 3, the strain required for failure in the model is also reduced upon saturation with water. Guided by our experimental data, we used a bulk density of 2550 and 1900  $\text{kg}/\text{m}^3$  for unaltered and altered wet rocks, respectively. Finally, we highlight that, although alteration is thought to have reduced the strength of the dome rocks from La Soufrière de Guadeloupe (Fig. 4b; see also discussions in Heap et al., 2021a, 2022a), alteration has also been observed, or inferred, to increase the strength of volcanic rocks (e.g., Frolova et al., 2014; Pola et al., 2014; Wyering et al., 2014; Coats et al., 2018; Heap et al., 2020b, 2021b; Kanakiya et al., 2021, 2022). Although the rocks in these studies contain minerals such as kaolinite and alunite, minerals that may promote water-weakening, it is unclear at present whether volcanic rocks that exhibit a strengthening resulting from alteration would be, as seen for the rocks from La Soufrière de Guadeloupe (Figs. 4, 5, 6, and 8), weaker in the presence of water. As a result, until new experimental data are available, the numerical modelling presented herein should be considered applicable for scenarios in which alteration reduces strength.

The results of the modelling show that displacements across the unaltered dome are essentially zero when the dome is water-saturated (Fig. 10b), suggesting that water-saturation alone does not significantly influence the stability of an unaltered dome. By contrast, displacements are high (up to 0.5 m) when the altered dome is water-saturated, with the highest displacements concentrated at the centre of the dome (Fig. 10d). Therefore, if an altered dome becomes saturated by, for example, heavy rainfall or rising hydrothermal fluids, the stability of the dome could be compromised, potentially promoting mass-wasting events (e.g., partial dome collapse). We highlight that the propensity for such an altered water saturated dome to collapse will likely be significantly enhanced if the dome is resting on a sloping substratum (see, for example, Harnett and Heap, 2021) or comprises listric low-

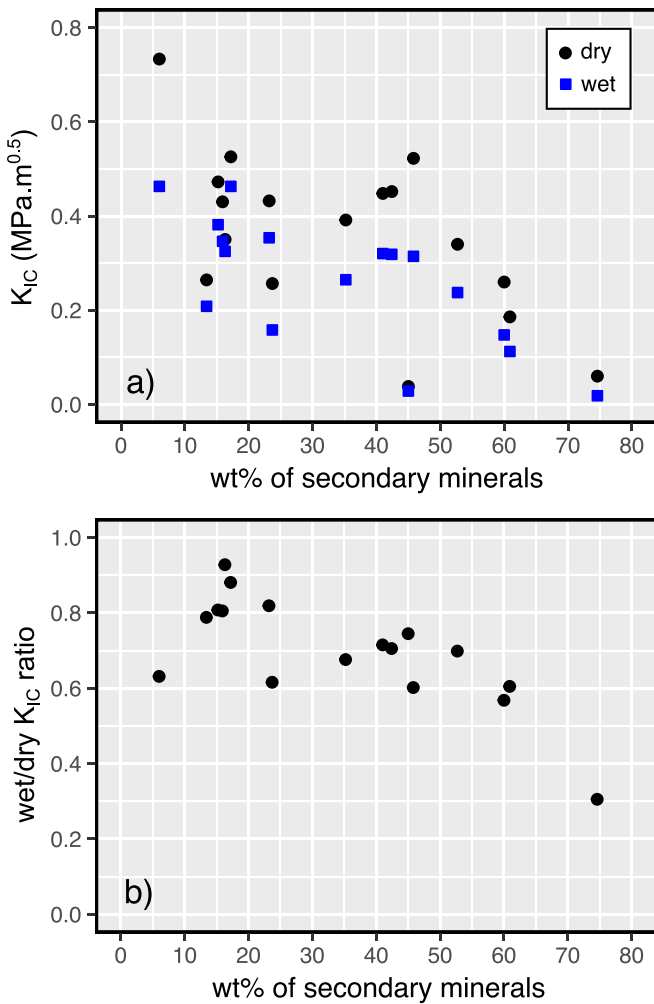


**Fig. 9.** (a) Fracture toughness ( $K_{IC}$ ) and (b) the wet to dry  $K_{IC}$  ratio as a function of the wt% of secondary minerals (i.e. alteration) for samples from La Soufrière de Guadeloupe (Eastern Caribbean). Values of  $K_{IC}$  are estimated using the analytical approximation of Sammis and Ashby (1986) pore-emitting crack micromechanical model provided by Zhu et al. (2010) (Eq. (1)). The relative uncertainties in the quantification of the mineral contents (Table 1) are on the order of 5–10%.

strength layers from previous partial flank collapses that are opened in the direction of maximum slope.

The scenarios shown in Fig. 10 represent end-member scenarios in which the dome is either completely unaltered or completely altered. In nature, hydrothermal alteration is likely to be heterogeneously distributed within a dome (e.g., along permeable discontinuities). Therefore, we performed additional modelling in which we included a buried altered zone within an otherwise unaltered dome (Fig. 11). In the first scenario, both the unaltered and altered regions were dry (Fig. 11b). In this scenario, only minor displacement is observed within and above the buried altered zone (Fig. 11b). In the second scenario, both the unaltered and altered regions were water-saturated (Fig. 11c). In this scenario, larger displacements are observed within the altered zone, and notable displacements are also observed on the half of the dome containing the buried alteration zone (Fig. 11c). In other words, dome instability was exacerbated following saturation in the presence of hydrothermally altered materials. Therefore, the stability of a dome can be compromised by water-saturation (e.g., heavy rainfall, changes to the hydrothermal system, and/or influx of seawater) even when only a small portion of the dome is hydrothermally altered. It is likely, in this scenario, that dome stability would be compromised more by alteration zones at or near the

base of the dome, rather than at the top of the dome.

The results of our modelling (Figs. 10 and 11) may help explain why the frequency of landslides and the failure and collapse of volcanic slopes and domes increases following heavy rainfall (Kerle and De Vries, 2001; Matthews et al., 2002; Matthews and Barclay, 2004; Elsworth et al., 2004; Simmons et al., 2004; Taron et al., 2007; Saucedo et al., 2008; Hicks et al., 2010; Vazquez et al., 2022).

Extreme or heavy rainfall has been linked to multiple volcanic hazards (McKee et al., 1981; Matthews et al., 2002; Barclay et al., 2006), with theorised mechanisms that range from deep-seated saturation and stress perturbations (McBirney, 1955; Violette et al., 2001; Farquharson and Amelung, 2020; Sahoo et al., 2022) to shallow-seated processes operating in the dome or upper edifice. Of these, the latter is often explained in terms of volumetric expansion of liquids as a function of fuel-coolant interactions (Elsworth et al., 2004; Simmons et al., 2004; Taron et al., 2007), with dome pressurisation and/or weakening driven by thermal stress mechanisms (i.e. contraction of the dome carapace; Mastin, 1994; Yamasato et al., 1998; Elsworth et al., 2004), or the stress on surrounding host-rock caused by the rapid growth of a dome or cryptodome at shallow depth (Voight et al., 1981, 2002; Young et al., 2002). More broadly, the saturation state of the edifice is thought to play an important role in volcano destabilisation (McGuire, 1996; Day, 1996; Delcamp et al., 2016; Ball et al., 2018; Finn et al., 2018; Heap et al., 2021b) and other failure processes, such as the failure of magma reservoirs (Albino et al., 2018). Large-scale sector collapse events are also thought to be facilitated by precipitation-induced retrogressive headward erosion and the weakening of former partial flank collapse slip surfaces following precipitation (Kerle and De Vries, 2001; Kerle et al., 2003; Capra, 2006; Tost and Cronin, 2016; Romero et al., 2021). Our new data presented here points to an additional role of dome or edifice rock saturation in promoting volcano instability, in that saturation with water results in a reduction of rock strength of ~10–60% (Fig. 5a).

The distribution and degree of hydrothermal alteration throughout a volcanic edifice is also thought to be key in determining the potential for collapse-related hazards. Commonly occurring hydrothermal mineral assemblages are thought to have a deleterious effect on volcano stability (López and Williams, 1993; Watters et al., 2000; van Wyk de Vries et al., 2000; Reid et al., 2001; Voight et al., 2002; Reid, 2004; Cecchi et al., 2004; Salaün et al., 2011; Ball et al., 2015; Detienne et al., 2017; Norini et al., 2020; Heap et al., 2021a), as supported by geomechanical studies on the role of hydrothermal alteration in reducing the strength of volcanic materials (in both natural and laboratory settings; Moon and Jayawardane, 2004; del Potro and Hürlimann, 2009; Pola et al., 2014; Wyering et al., 2014; Farquharson et al., 2019; Mordensky et al., 2019; Heap et al., 2021a, 2022a; Darmawan et al., 2022). Indeed, structural failure is often spatially coincident with hydrothermal alteration (Siebert et al., 1987; Delmelle et al., 2015); for example, Zimbelman (1996) notes the association of alteration minerals—including alunite, jarosite, and other sulphates—with exposed collapse scars, and Zimbelman et al. (2005) link collapse events at andesitic arc volcanoes to veins of alteration minerals resulting from the mixing of magmatic sulphate and meteoric water. Indeed, Voight et al. (2002) found varicoloured hydrothermally altered materials within avalanche deposits at Soufrière Hills volcano (Montserrat, Eastern Caribbean). This link is congruent with observations at La Soufrière de Guadeloupe, where avalanche deposits and material ejected during phreatic explosions were found to contain various parts of the active and ancient hydrothermal systems of the volcano (as evidenced by an acid-sulphate mineral assemblage; Salaün et al., 2011; Heap et al., 2021a), and collapse events have revealed visibly altered material beneath (see Fig. 1b). La Soufrière de Guadeloupe is characterised by a vigorous hydrothermal system (Komorowski et al., 2005; Villemant et al., 2005; Nicollin et al., 2006; Coutant et al., 2012; Lesparre et al., 2012; Brothelande et al., 2014; Villemant et al., 2014; Rosas-Carbajal et al., 2016, 2017; Moretti et al., 2020; Gibert et al., 2022) and, notably, weathering fluxes on the volcano are among the highest recorded in tropical volcanic settings (Dessert

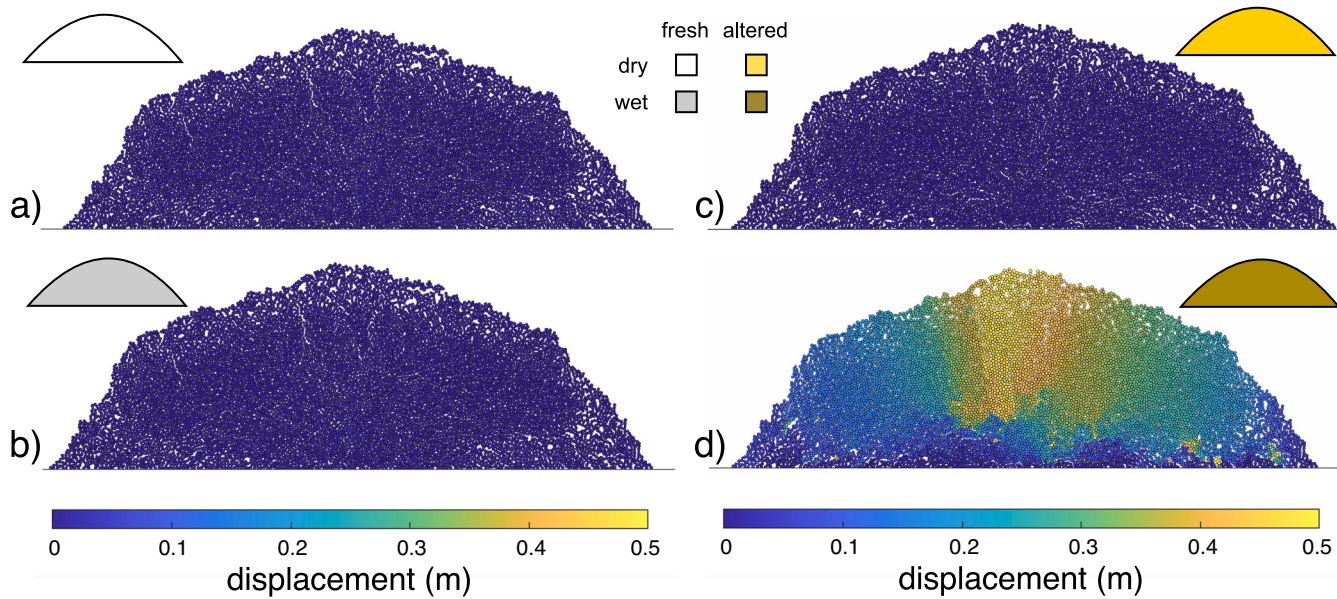


**Fig. 10.** A stable (i.e. no displacement) dome generated in Particle Flow Code (PFC) for a (a) dry unaltered dome and (c) dry altered dome. (b) The displacement in the dome shown in (a) resulting from changing the mechanical properties of the contacts in the stable dome to represent wet unaltered rock. (d) The displacement in the dome shown in (c) resulting from changing the mechanical properties of the contacts to represent wet altered rock. Blue - low displacement; yellow - high displacement.

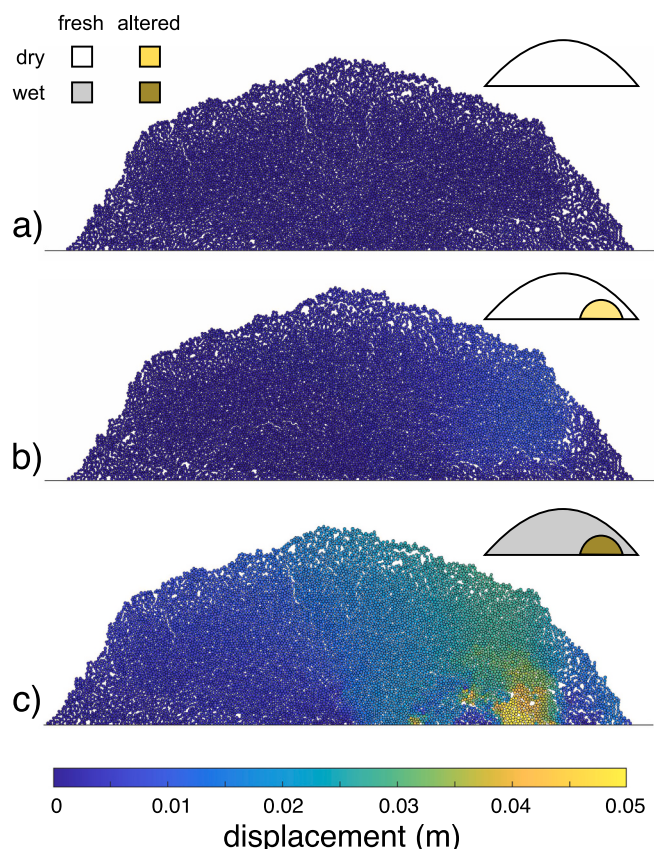


**Fig. 11.** (a) Stable (i.e. no displacement) dry altered dome generated in Particle Flow Code (PFC). (b) The displacement in the dome shown in (a) resulting from adding a buried dry alteration zone within a dry unaltered dome (as in Harnett et al., 2022). (c) The displacement in the dome shown in (a) resulting from adding a buried wet alteration zone within a wet unaltered dome. Blue - low displacement; yellow - high displacement. (For interpretation of the references to colour in this figure legend, the reader is referred to the web version of this article.)

et al., 2015). Our new data underscore the importance of this hydrothermal alteration on the mechanical properties of dome-forming rocks (Fig. 5b), with UCS decreasing by as much as ~60% upon water-saturation for highly altered materials (i.e. with a high proportion of secondary minerals). These data further highlight how and why hydrothermal alteration and water (meteoric, hydrothermal, or seawater) conspire to destabilise volcanic structures, as outlined in disastrous effect by the 1998 collapse at Casita volcano (van Wyk de Vries et al., 2000; Kerle and De Vries, 2001; Kerle et al., 2003; Opfergelt et al., 2006) and several large rain-triggered collapses during the period of active dome growth at Soufrière Hills volcano (Elsworth et al., 2004; Simmons et al., 2004; Taron et al., 2007).

Based on observations of rainfall-induced dome instability at Soufrière Hills volcano, previous research has focussed on developing mechanistic models of dome collapse as a function of local rainfall rate (Elsworth et al., 2004; Matthews and Barclay, 2004; Taron et al., 2007; see also Harnett et al., 2019) thereby—directly or indirectly—accounting for the saturation state. In contrast, numerous studies that model the influence of alteration on dome or flank stability do not consider the presence or absence of interstitial fluids on the mechanical properties of the dome-forming materials. Critically, our modelling results (Figs. 10 and 11) demonstrate that mechanical failure is promoted when both hydrothermal alteration and water-saturation operate in tandem. We emphasise that mechanical water-weakening is an important additional mechanism that has generally not been considered in existing stability modelling of domes, but that can facilitate collapse, particularly in the likely scenario when alteration is also present (Figs. 10 and 11). We suggest that, when appropriate and where available, volcano stability models use data relevant for water-saturated volcanic rocks. We consider this especially relevant for submarine, coastal, and ocean-island volcanoes. For the modelling of coastal and ocean-island volcanoes, it is likely important to not only consider the partially saturated subaerial part of the volcano, but also the saturated submarine part (the importance of not neglecting the submarine portion of a coastal volcano is discussed in Urlaub et al., 2018).

We also highlight that the link between mechanical water-weakening and hydrothermal alteration may also be further exacerbated when hot gases and rising hydrothermal/magmatic fluids interact with water-saturated altered zones at shallow levels within a dome or

volcano, generating large volumes of steam and elevated fluid pore pressures. Indeed, previous modelling has shown that elevated pore pressure negatively impacts volcano stability (Reid, 2004; Heap et al., 2021b). The rise of large volumes of hydrothermal fluids due to major heat pulses was observed during all phreatic unrest and eruptions at La Soufrière of Guadeloupe (Komorowski et al., 2005; Rosas-Carbajal et al., 2016) and Mount Pelée in 1902 (Tanguy, 1994), and is characteristic of the ongoing unrest at La Soufrière of Guadeloupe (Moretti et al., 2020), underscoring the importance of incorporating these phenomena into future, more complex volcano stability models.

By combining our experimental results with analytical and numerical mechanical modelling, we link the micro-scale effects of hydrothermal alteration on the fracture mechanics to the scale of the dome. These considerations are particularly important in light of projected climate futures (Aubry et al., 2022). As circulation models results in Fig. 1c highlight, La Soufrière de Guadeloupe is projected to receive increasing amounts of heavy rainfall over the next 80 years (see also Cantet et al., 2014), even given widespread adoption of stringent climate change mitigation policies. Accordingly, the propensity for rainfall-induced collapse events will likely increase as well, and detecting where potential collapse events may occur becomes ever more crucial, especially given the absence of detectable geophysical signals preceding such events (Matthews et al., 2002). Our model results highlight that identifying zones of (potentially concealed) hydrothermal alteration may prove to be key in mitigating such hazards (Darmawan et al., 2022; Harnett et al., 2022). Moreover, our results emphasise that close monitoring of domes and slopes during and following heavy rainfall is essential: we echo the call of Barclay et al. (2006) for routine incorporation of meteorological data into monitoring praxis. Finally, direct knowledge of the state of edifice or dome saturation could be invaluable for future stability monitoring. Our new data and models add a new importance to the 3D characterisation of water saturation in volcanic edifices, as well as its evolution over time, using geophysical methods. For example, geophysical methods such as electrical resistivity tomography (e.g., Rosas-Carbajal et al., 2016) and muon tomography (Rosas-Carbajal et al., 2017; Bajou et al., 2023) are sensitive to water content and could be repeatedly employed to assess the distribution of water in the upper parts of the volcanic edifice. Both seismic noise interferometry (Sens-Schönfelder and Wegler, 2006), a method increasingly used to monitor water level variations, and the satellite-based monitoring of groundwater (Rodell et al., 2009) could also be powerful tools to track edifice or dome saturation. Finally, borehole dilatometers and piezometers (Hurwitz and Johnston, 2003) could provide punctual and precise data to calibrate numerical models and interpret geophysical imaging.

While La Soufrière de Guadeloupe has been chosen as a case study herein, for the reasons outlined in section two, we emphasise that our conclusions are much more broadly applicable. Volcanoes exhibiting zones of intense alteration and/or vigorous hydrothermal systems (Africano and Bernard, 2000; Zimbelman et al., 2005; Rodríguez and van Bergen, 2017; Yilmaz et al., 2021), as well as those with persistent acid lakes (van Hinsberg et al., 2010; Rouwet et al., 2014; Delmelle et al., 2015), will likely be particularly prone to extensive water-weakening, and therefore heightened instability, in the event of edifice and/or dome saturation. In tropical environments, increasingly frequent bouts of intense precipitation (not only during the so-called hurricane or rainy season but also at other times of the year in the Tropics) may directly trigger mass-wasting events (as observed elsewhere in the Caribbean: Matthews et al., 2002; Carn et al., 2004; Taron et al., 2007; Matthews et al., 2009 and in other settings: Yamasato et al., 1998; Elsworth et al., 2004), or facilitate other internal or external trigger mechanisms such as magma movement (Reid et al., 2010), pressurisation (Reid, 2004; Heap et al., 2021b), or basal spreading (van Wyk de Vries and Francis, 1997). For the majority of subaerial volcanoes, climate models project an increase in such meteorological events (Farquharson and Amelung, 2022). In the context of water-weakening and related hazards, climate change may also be important

in terms of sea level rise. Analysis of drill cores from offshore Montserrat shows that Soufrière Hills volcano underwent periods of heightened instability during periods of rapid sea level rise, with all three large collapse events at the volcano being correlated with sea level changes of >5 m/ka (Coussens et al., 2016); those authors also highlight that this phenomenon appears to echo a broader trend across other island arc volcanoes. We further posit that variation in edifice saturation due to sea level rise could also promote instability in coastal or island arc volcanoes.

## 6. Conclusions

The goal of this study, using dome stability models informed by experimental data, was to investigate whether water-saturation alone can jeopardise the stability of a lava dome. Our experiments show that water-saturation reduced the strength of variably-altered dome rocks, and that water-weakening increased as the degree of alteration increased. Micromechanical modelling suggested that the observed water-weakening was the result of a decrease in fracture toughness,  $K_{IC}$ , in the presence of water. The ratio of wet to dry  $K_{IC}$  also decreased with increasing alteration, explaining the trend of increasing water-weakening with increasing alteration. Dome stability modelling, informed by our experimental data, showed that the stability of a lava dome can be compromised by water-saturation if the dome is altered, or contains an altered zone (even without the compounding exacerbating effects of volcanic unrest, such as seismicity, deformation, high heat fluxes, and rising fluids). The models presented herein may therefore help explain why the frequency of landslides and the failure and collapse of altered volcanic slopes and dome increases following heavy rainfall. Our study highlights, and especially in the light of predicted increases in heavy rainfall due to climate change, that the degree of alteration and water-saturation should be monitored at active volcanoes worldwide, volcanic domes and slopes should be closely monitored following heavy rainfall, and that large-scale volcano stability models should use values for water-saturated rocks where and when appropriate.

## CRediT authorship contribution statement

**Michael J. Heap:** Conceptualization, Methodology, Formal analysis, Investigation, Resources, Writing – original draft, Writing – review & editing, Visualization, Project administration, Funding acquisition. **Claire Harnett:** Conceptualization, Methodology, Software, Formal analysis, Investigation, Resources, Writing – original draft, Writing – review & editing, Visualization, Funding acquisition. **Jamie Farquharson:** Formal analysis, Writing – original draft, Writing – review & editing, Visualization. **Patrick Baud:** Formal analysis, Writing – review & editing. **Marina Rosas-Carbajal:** Writing – review & editing. **Jean-Christophe Komorowski:** Writing – review & editing. **Marie E.S. Violay:** Resources, Writing – review & editing, Funding acquisition. **H. Albert Gilg:** Resources, Writing – review & editing. **Thierry Reuschlé:** Writing – review & editing.

## Declaration of Competing Interest

The authors declare that they have no known competing financial interests or personal relationships that could have appeared to influence the work reported in this paper.

## Data availability

The data are given in the tables in the manuscript.

## Acknowledgements

This work was supported by ANR grant MYGALÉ ("Modelling the phYsical and chemical Gradients of hydrothermal ALteration for

warning systems of flank collapse at Explosive volcanoes"; ANR-21-CE49-0010). M. Heap also acknowledges support from the Institut Universitaire de France (IUF). We thank Tomaso Esposti Ongaro and Lucille Carbillet for help in the field, Laurent Gastaldo and Bertrand Renaudie for help in the laboratory, and all those working at the Observatoire Volcanologique et Sismologique de Guadeloupe (OVSG). This research was also supported by two Hubert Curien Partnership (PHC) grants: a Germaine de Staël grant awarded to M. Heap and M. Violay (grant number 47712SB) and a Ulysses grant awarded to M. Heap and C. Harnett (grant number 47199ZM). The Germaine de Staël grant is implemented by the Ministry for Higher Education, Research, and Innovation (MESRI) and the Ministry for Europe and Foreign Affairs (MEAE) in France, and by the State Secretariat for Education, Research, and Innovation (SERI) and the Swiss Academy of Technical Sciences (SATW) in Switzerland. The Ulysses grant is implemented by the MEAE and the MESRI in France, and by the Irish Research Council (IRC) in Ireland. This research also benefitted from European Research Council Starting Grant BEFINE (ERC-2017-STG), awarded to M. Violay. We thank the IPGP for general funding for the Observatoires Volcanologiques et Sismologiques (OVS), INSU-CNRS for the funding provided to the Service National d'Observation en Volcanologie (SNOV), and the Ministère pour la Transition Ecologique (MTE) for financial support for the monitoring of the unstable flank of La Soufrière de Guadeloupe. We are grateful to the Parc National de la Guadeloupe for allowing us to carry out geological fieldwork on La Soufrière de Guadeloupe. Finally, we thank The Fleet (Dublin, Ireland) for their hospitality. The constructive comments of Shane Cronin, Ludmila Adam, and Anthony Lamur helped improve this manuscript.

## Appendix A. Supplementary data

Supplementary data to this article can be found online at <https://doi.org/10.1016/j.jvolgeores.2023.107962>.

## References

- Africano, F., Bernard, A., 2000. Acid alteration in the fumarolic environment of Usu volcano, Hokkaido, Japan. *J. Volcanol. Geotherm. Res.* 97 (1–4), 475–495.
- Aizawa, K., Ogawa, Y., Ishido, T., 2009. Groundwater flow and hydrothermal systems within volcanic edifices: Delineation by electric self-potential and magnetotellurics. *J. Geophys. Res. Solid Earth* 114 (B1).
- Albino, F., Amelung, F., Gregg, P., 2018. The role of pore fluid pressure on the failure of magma reservoirs: insights from Indonesian and Aleutian arc volcanoes. *J. Geophys. Res. Solid Earth* 123 (2), 1328–1349.
- Allemand, P., Delacourt, C., Lajeunesse, E., Devauchelle, O., Beauducel, F., 2014. Erosive effects of the storm Helene (1963) on Basse Terre Island (Guadeloupe—Lesser Antilles Arc). *Geomorphology* 206, 79–86.
- Apuani, T., Corazzato, C., Cancelli, A., Tibaldi, A., 2005. Stability of a collapsing volcano (Stromboli, Italy): Limit equilibrium analysis and numerical modelling. *J. Volcanol. Geotherm. Res.* 144 (1–4), 191–210.
- Atkinson, B.K., 1984. Subcritical crack growth in geological materials. *J. Geophys. Res. Solid Earth* 89 (B6), 4077–4114.
- Aubry, T.J., Farquharson, J.I., Rowell, C.R., Watt, S.F., Pinel, V., Beckett, F., Sykes, J.S., 2022. Impact of climate change on volcanic processes: current understanding and future challenges. *Bull. Volcanol.* 84 (6), 58.
- Bajou, R., Rosas-Carbajal, M., Tonazzo, A., Marteau, J., 2023. High-resolution structural imaging of volcanoes using improved muon tracking. *Geophys. J. Int.* 235 (2), 1138–1149.
- Ball, J.L., Stauffer, P.H., Calder, E.S., Valentine, G.A., 2015. The hydrothermal alteration of cooling lava domes. *Bull. Volcanol.* 77, 1–16.
- Ball, J.L., Taron, J., Reid, M.E., Hurwitz, S., Finn, C., Bedrosian, P., 2018. Combining multiphase groundwater flow and slope stability models to assess stratovolcano flank collapse in the Cascade Range. *J. Geophys. Res. Solid Earth* 123 (4), 2787–2805.
- Barclay, J., Johnstone, J.E., Matthews, A.J., 2006. Meteorological monitoring of an active volcano: implications for eruption prediction. *J. Volcanol. Geotherm. Res.* 150 (4), 339–358.
- Baud, P., Zhu, W., Wong, T.F., 2000. Failure mode and weakening effect of water on sandstone. *J. Geophys. Res. Solid Earth* 105 (B7), 16371–16389.
- Baud, P., Reuschlé, T., Ji, Y., Cheung, C.S., Wong, T.F., 2015. Mechanical compaction and strain localization in Bleurswiller sandstone. *J. Geophys. Res. Solid Earth* 120 (9), 6501–6522.
- Baud, P., Rolland, A., Heap, M., Xu, T., Nicló, M., Ferrand, T., Conil, N., 2016. Impact of stylolites on the mechanical strength of limestone. *Tectonophysics* 690, 4–20.
- Borselli, L., Capra, L., Sarocchi, D., De la Cruz-Reyna, S., 2011. Flank collapse scenarios at Volcán de Colima, Mexico: a relative instability analysis. *J. Volcanol. Geotherm. Res.* 208 (1–2), 51–65.
- Boudon, G., Komorowski, J.C., Villemant, B., Semet, M.P., 2008. A new scenario for the last magmatic eruption of La Soufrière of Guadeloupe (Lesser Antilles) in 1530 AD evidence from stratigraphy radiocarbon dating and magmatic evolution of erupted products. *J. Volcanol. Geotherm. Res.* 178 (3), 474–490.
- Brantut, N., Heap, M.J., Meredith, P.G., Baud, P., 2013. Time-dependent cracking and brittle creep in crustal rocks: A review. *J. Struct. Geol.* 52, 17–43.
- Brombach, T., Marini, L., Hunziker, J.C., 2000. Geochemistry of the thermal springs and fumaroles of Basse-Terre Island, Guadeloupe, Lesser Antilles. *Bull. Volcanol.* 61, 477–490.
- Brothelande, E., Finizola, A., Peltier, A., Delcher, E., Komorowski, J.C., Di Gangi, F., Legendre, Y., 2014. Fluid circulation pattern inside La Soufrière volcano (Guadeloupe) inferred from combined electrical resistivity tomography, self-potential, soil temperature and diffuse degassing measurements. *J. Volcanol. Geotherm. Res.* 288, 105–122.
- Cantet, P., Déqué, M., Palany, P., Maridet, J.L., 2014. The importance of using a high-resolution model to study the climate change on small islands: the Lesser Antilles case. *Tellus A: Dynam. Meteorol. Oceanogr.* 66 (1), 24065.
- Capra, L., 2006. Abrupt climatic changes as triggering mechanisms of massive volcanic collapses. *J. Volcanol. Geotherm. Res.* 155 (3–4), 329–333.
- Carn, S.A., Watts, R.B., Thompson, G., Norton, G.E., 2004. Anatomy of a lava dome collapse: the 20 March 2000 event at Soufrière Hills Volcano, Montserrat. *J. Volcanol. Geotherm. Res.* 131 (3–4), 241–264.
- Carr, B.B., Lev, E., Vanderklutsen, L., Moyer, D., Marlyani, G.I., Clarke, A.B., 2022. The stability and collapse of lava domes: Insight from photogrammetry and slope stability models applied to Sinabung volcano (Indonesia). *Front. Earth Sci.* 10, 813813.
- Caselle, C., Baud, P., Kushnir, A.R.L., Reuschlé, T., Bonetto, S.M.R., 2022. Influence of water on deformation and failure of gypsum rock. *J. Struct. Geol.* 163, 104722.
- Castagna, A., Ougier-Simonin, A., Benson, P.M., Browning, J., Walker, R.J., Fazio, M., Vinciguerra, S., 2018. Thermal damage and pore pressure effects of the Brittle-Ductile transition in comiso limestone. *J. Geophys. Res. Solid Earth* 123 (9), 7644–7660.
- Ceccchi, E., van Wyk de Vries, B., Lavest, J.M., 2004. Flank spreading and collapse of weak-cored volcanoes. *Bull. Volcanol.* 67, 72–91.
- Chester, F.M., Logan, J.M., 1986. Implications for mechanical properties of brittle faults from observations of the Punchbowl fault zone, California. *Pure Appl. Geophys.* 124, 79–106.
- Coats, R., Kendrick, J.E., Wallace, P.A., Miwa, T., Hornby, A.J., Ashworth, J.D., Lavallée, Y., 2018. Failure criteria for porous dome rocks and lavas: a study of Mt. Unzen, Japan. *Solid Earth* 9, 1299–1328.
- Coussens, M., Wall-Palmer, D., Talling, P.J., Watt, S.F., Cassidy, M., Jutzeler, M., Stinton, A.J., 2016. The relationship between eruptive activity, flank collapse, and sea level at volcanic islands: A long-term (> 1 Ma) record offshore Montserrat, Lesser Antilles. *Geochem. Geophys. Geosyst.* 17 (7), 2591–2611.
- Coutant, O., Bernard, M.L., Beauducel, F., Nicolin, F., Bouin, M.P., Roussel, S., 2012. Joint inversion of P-wave velocity and density, application to La Soufrière de Guadeloupe hydrothermal system. *Geophys. J. Int.* 191 (2), 723–742.
- Darmawan, H., Troll, V.R., Walter, T.R., Deegan, F.M., Geiger, H., Heap, M.J., Müller, D., 2022. Hidden mechanical weaknesses within lava domes provided by buried high-porosity hydrothermal alteration zones. *Sci. Rep.* 12 (1), 3202.
- Day, S.J., 1996. Hydrothermal pore fluid pressure and the stability of porous, permeable volcanoes. *Geol. Soc. Lond. Spec. Publ.* 110 (1), 77–93.
- de Bremon d'Ars, J., Gibert, D., 2022. Multiscale external rainfall forcing from high-resolution temperature time series of fumaroles at La Soufrière de Guadeloupe volcano. *Front. Earth Sci.* 9, 1364.
- del Potro, R., Hürlimann, M., 2009. The decrease in the shear strength of volcanic materials with argillic hydrothermal alteration, insights from the summit region of Teide stratovolcano, Tenerife. *Eng. Geol.* 104 (1–2), 135–143.
- Delcamp, A., Roberti, G., van Wyk de Vries, B., 2016. Water in volcanoes: evolution, storage and rapid release during landslides. *Bull. Volcanol.* 78, 1–12.
- Delmelle, P., Bernard, A., Kusakabe, M., Fischer, T.P., Takano, B., 2000. Geochemistry of the magmatic-hydrothermal system of Kawah Ijen volcano, East Java, Indonesia. *J. Volcanol. Geotherm. Res.* 97 (1–4), 31–53.
- Delmelle, P., Henley, R.W., Opfergelt, S., Detienne, M., 2015. Summit acid crater lakes and flank instability in composite volcanoes. *Volcanic Lakes* 289–305.
- Dessert, C., Lajeunesse, E., Lloret, E., Clergue, C., Crispé, O., Gorge, C., Quidelleur, X., 2015. Controls on chemical weathering on a mountainous volcanic tropical island: Guadeloupe (French West Indies). *Geochim. Cosmochim. Acta* 171, 216–237.
- Detienne, M., Delmelle, P., Guevara, A., Samaniego, P., Opfergelt, S., Mothes, P.A., 2017. Contrasting origin of two clay-rich debris flows at Cayambe Volcanic Complex, Ecuador. *Bull. Volcanol.* 79, 1–14.
- Duda, M., Renner, J., 2013. The weakening effect of water on the brittle failure strength of sandstone. *Geophys. J. Int.* 192 (3), 1091–1108.
- Elsworth, D., Voight, B., Thompson, G., Young, S.R., 2004. Thermal-hydrologic mechanism for rainfall-triggered collapse of lava domes. *Geology* 32 (11), 969–972.
- Farquharson, J.I., Amelung, F., 2020. Extreme rainfall triggered the 2018 rift eruption at Kilauea Volcano. *Nature* 580 (7804), 491–495.
- Farquharson, J.I., Amelung, F., 2022. Volcanic hazard exacerbated by future global warming-driven increase in heavy rainfall. *R. Soc. Open Sci.* 9 (7), 220275.
- Farquharson, J.I., Wild, B., Kushnir, A.R., Heap, M.J., Baud, P., Kennedy, B., 2019. Acid-induced dissolution of andesite: evolution of permeability and strength. *J. Geophys. Res. Solid Earth* 124 (1), 257–273.

- Finn, C.A., Deszcz-Pan, M., Ball, J.L., Bloss, B.J., Minsley, B.J., 2018. Three-dimensional geophysical mapping of shallow water saturated altered rocks at Mount Baker, Washington: implications for slope stability. *J. Volcanol. Geotherm. Res.* 357, 261–275.
- Frolova, J., Ladygin, V., Rychagov, S., Zukhubaya, D., 2014. Effects of hydrothermal alterations on physical and mechanical properties of rocks in the Kuril-Kamchatka island arc. *Eng. Geol.* 183, 80–95.
- Frolova, J.V., Chernov, M.S., Rychagov, S.N., Ladygin, V.M., Sokolov, V.N., Kuznetsov, R.A., 2021. The influence of hydrothermal argillization on the physical and mechanical properties of tuffaceous rocks: a case study from the Upper Pauzhetsky thermal field, Kamchatka. *Bull. Eng. Geol. Environ.* 80, 1635–1651.
- Fulignati, P., 2020. Clay minerals in hydrothermal systems. *Minerals* 10 (10), 919.
- Gibert, D., de Bremond d'Ar, J., Carlos, B., Deroussi, S., Ianigro, J.C., Jessop, D.E., Rosas-Carbajal, M., 2022. Observation of the dynamics of hydrothermal activity in la soufrière de guadeloupe volcano with joint muography, gravimetry, electrical resistivity tomography, seismic and temperature monitoring. *Muography: Expl. Earth's Subsurf. Element. Part.* 55–73.
- Guha Roy, D., Singh, T.N., Kodikara, J., Talukdar, M., 2017. Correlating the mechanical and physical properties with mode-I fracture toughness of rocks. *Rock Mech. Rock Eng.* 50, 1941–1946.
- Harnett, C.E., Heap, M.J., 2021. Mechanical and topographic factors influencing lava dome growth and collapse. *J. Volcanol. Geotherm. Res.* 420, 107398.
- Harnett, C.E., Thomas, M.E., Purvance, M.D., Neuberg, J., 2018. Using a discrete element approach to model lava dome emplacement and collapse. *J. Volcanol. Geotherm. Res.* 359, 68–77.
- Harnett, C.E., Kendrick, J.E., Lamur, A., Thomas, M.E., Stanton, A., Wallace, P.A., Lavallée, Y., 2019. Evolution of mechanical properties of lava dome rocks across the 1995–2010 eruption of soufrière hills volcano, Montserrat. *Front. Earth Sci.* 7, 7.
- Harnett, C.E., Heap, M.J., Troll, V.R., Deegan, F.M., Walter, T.R., 2022. Large-scale lava dome fracturing as a result of concealed weakened zones. *Geology* 50 (12), 1346–1350.
- Hawkins, A.B., McConnell, B.J., 1992. Sensitivity of sandstone strength and deformability to changes in moisture content. *Q. J. Eng. Geol.* 25 (2), 115–130.
- Heap, M.J., Violay, M.E., 2021. The mechanical behaviour and failure modes of volcanic rocks: a review. *Bull. Volcanol.* 83 (5), 33.
- Heap, M.J., Kennedy, B.M., Pernin, N., Jacquemard, L., Baud, P., Farquharson, J.I., Dingwell, D.B., 2015. Mechanical behaviour and failure modes in the Whakaari (White Island volcano) hydrothermal system, New Zealand. *J. Volcanol. Geotherm. Res.* 295, 26–42.
- Heap, M.J., Farquharson, J.I., Kushnir, A.R., Lavallée, Y., Baud, P., Gilg, H.A., Reuschlé, T., 2018. The influence of water on the strength of Neapolitan Yellow Tuff, the most widely used building stone in Naples (Italy). *Bull. Volcanol.* 80, 1–15.
- Heap, M.J., Villeneuve, M., Kushnir, A.R., Farquharson, J.I., Baud, P., Reuschlé, T., 2019. Rock mass strength and elastic modulus of the Buntsandstein: an important lithostratigraphic unit for geothermal exploitation in the Upper Rhine Graben. *Geothermics* 77, 236–256.
- Heap, M.J., Villeneuve, M., Albino, F., Farquharson, J.I., Brothelande, E., Amelung, F., Baud, P., 2020a. Towards more realistic values of elastic moduli for volcano modelling. *J. Volcanol. Geotherm. Res.* 390, 106684.
- Heap, M.J., Gravley, D.M., Kennedy, B.M., Gilg, H.A., Bertolett, E., Barker, S.L., 2020b. Quantifying the role of hydrothermal alteration in creating geothermal and epithermal mineral resources: the Ohakuri ignimbrite (Taupo Volcanic Zone, New Zealand). *J. Volcanol. Geotherm. Res.* 390, 106703.
- Heap, M.J., Baumann, T.S., Rosas-Carbajal, M., Komorowski, J.C., Gilg, H.A., Villeneuve, M., Reuschlé, T., 2021a. Alteration-Induced Volcano Instability at La Soufrière de Guadeloupe (Eastern Caribbean). *J. Geophys. Res. Solid Earth* 126 (8), e2021JB022514.
- Heap, M.J., Baumann, T., Gilg, H.A., Kolzenburg, S., Ryan, A.G., Villeneuve, M., Clyne, M.A., 2021b. Hydrothermal alteration can result in pore pressurization and volcano instability. *Geology* 49 (11), 1348–1352.
- Heap, M.J., Harnett, C.E., Wadsworth, F.B., Gilg, H.A., Carbillot, L., Rosas-Carbajal, M., Moretti, R., 2022a. The tensile strength of hydrothermally altered volcanic rocks. *J. Volcanol. Geotherm. Res.* 428, 107576.
- Heap, M.J., Jessop, D.E., Wadsworth, F.B., Rosas-Carbajal, M., Komorowski, J.C., Gilg, H.A., Moretti, R., 2022b. The thermal properties of hydrothermally altered andesites from La Soufrière de Guadeloupe (Eastern Caribbean). *J. Volcanol. Geotherm. Res.* 421, 107444.
- Heap, M.J., Troll, V.R., Harris, C., Gilg, H.A., Moretti, R., Rosas-Carbajal, M., Baud, P., 2022c. Whole-rock oxygen isotope ratios as a proxy for the strength and stiffness of hydrothermally altered volcanic rocks. *Bull. Volcanol.* 84 (8), 74.
- Heap, M.J., Harnett, C.E., Nazarbayov, T., Heng, Z., Baud, P., Xu, T., Komorowski, J.C., 2023a. The influence of heterogeneity on the strength of volcanic rocks and the stability of lava domes. *Bull. Volcanol.* 85 (9), 49.
- Heap, M.J., Wadsworth, F.B., Jessop, D.E., 2023b. The thermal conductivity of un lithified granular volcanic materials: the influence of hydrothermal alteration and degree of water saturation. *J. Volcanol. Geotherm. Res.* 107775.
- Hicks, P.D., Matthews, A.J., Cooker, M.J., 2010. Triggering of a volcanic dome collapse by rainwater infiltration. *J. Geophys. Res. Solid Earth* 115 (B9).
- Hurwitz, S., Johnston, M.J., 2003. Groundwater level changes in a deep well in response to a magma intrusion event on Kilauea Volcano, Hawai'i. *Geophys. Res. Lett.* 30 (22) <https://doi.org/10.1029/2003GL018676>.
- Hurwitz, S., Kipp, K.L., Ingebritsen, S.E., Reid, M.E., 2003. Groundwater flow, heat transport, and water table position within volcanic edifices: Implications for volcanic processes in the Cascade Range. *J. Geophys. Res. Solid Earth* 108 (B12).
- Husain, T., Elsworth, D., Voight, B., Mattioli, G., Jansma, P., 2014. Influence of extrusion rate and magma rheology on the growth of lava domes: Insights from particle-dynamics modeling. *J. Volcanol. Geotherm. Res.* 285, 100–117.
- Husain, T., Elsworth, D., Voight, B., Mattioli, G., Jansma, P., 2018. Influence of conduit flow mechanics on magma rheology and the growth style of lava domes. *Geophys. J. Int.* 213 (3), 1768–1784.
- Husain, T., Elsworth, D., Voight, B., Mattioli, G., Jansma, P., 2019. Morphologic variation of an evolving dome controlled by the extrusion of finite yield strength magma. *J. Volcanol. Geotherm. Res.* 370, 51–64.
- Inoue, A., 1995. Formation of clay minerals in hydrothermal environments. *Origin Mineral. Clays: Clays Environ.* 268–329.
- Jessop, D.E., Moune, S., Moretti, R., Gibert, D., Komorowski, J.C., Robert, V., Burtin, A., 2021. A multi-decadal view of the heat and mass budget of a volcano in unrest: La Soufrière de Guadeloupe (French West Indies). *Bull. Volcanol.* 83, 1–19.
- Join, J.L., Folio, J.L., Robinet, B., 2005. Aquifers and groundwater within active shield volcanoes. Evolution of conceptual models in the Piton de la Fournaise volcano. *J. Volcanol. Geotherm. Res.* 147 (1–2), 187–201.
- Kanakiya, S., Adam, L., Rowe, M.C., Lindsay, J.M., Esteban, L., 2021. The role of tuffs in sealing volcanic conduits. *Geophys. Res. Lett.* 48 (20), e2021GL095175.
- Kanakiya, S., Adam, L., Rowe, M.C., Esteban, L., Lerner, G.A., Lindsay, J.M., 2022. Petrophysical and elastic properties of altered lavas from Mt. Taranaki: Implications for dome stability. *J. Volcanol. Geotherm. Res.* 432, 107693.
- Kataoka, M., Obara, Y., Kuruppu, M., 2015. Estimation of fracture toughness of anisotropic rocks by semi-circular bend (SCB) tests under water vapor pressure. *Rock Mech. Rock Eng.* 48, 1353–1367.
- Kendrick, J.E., Schaefer, L.N., Schauroth, J., Bell, A.F., Lamb, O.D., Lamur, A., Kennedy, B.M., 2021. Physical and mechanical rock properties of a heterogeneous volcano: the case of Mount Unzen, Japan. *Solid Earth* 12 (3), 633–664.
- Kerle, N., De Vries, B.V.W., 2001. The 1998 debris avalanche at Casita volcano, Nicaragua—investigation of structural deformation as the cause of slope instability using remote sensing. *J. Volcanol. Geotherm. Res.* 105 (1–2), 49–63.
- Kerle, N., van Wyk de Vries, B., Oppenheimer, C., 2003. New insight into the factors leading to the 1998 flank collapse and lahar disaster at Casita volcano, Nicaragua. *Bull. Volcanol.* 65, 331–345.
- Komorowski, J.-C., Boudon, G., Semet, M., Beauducel, F., Antenor-Habazac, C., Bazin, S., Hammouya, G., 2005. Guadeloupe. In: Lindsay, J., Robertson, R., Shepherd, J., Ali, S. (Eds.), *Volcanic Atlas of the Lesser Antilles*. University of the French West Indies, Seismic Research Unit, pp. 65–102.
- Kranz, R.L., Harris, W.J., Carter, N.L., 1982. Static fatigue of granite at 200 °C. *Geophys. Res. Lett.* 9 (1), 1–4.
- Le Friant, A., Boudon, G., Komorowski, J.C., Heinrich, P., Semet, M.P., 2006. Potential flank-collapse of Soufrière Volcano, Guadeloupe, lesser Antilles? Numerical simulation and hazards. *Nat. Hazards* 39, 381–393.
- Legendre, Y., 2012. Reconstruction fine de l'histoire éruptive et scénarii éruptifs à la Soufrière de Guadeloupe : vers un modèle intégré de fonctionnement du volcan (Doctoral dissertation, Université Paris 7-Denis Diderot; Institut de Physique du Globe de Paris).
- Lesparre, N., Gibert, D., Marteau, J., Komorowski, J.C., Nicollin, F., Coutant, O., 2012. Density muon radiography of La Soufrière of Guadeloupe volcano: comparison with geological, electrical resistivity and gravity data. *Geophys. J. Int.* 190 (2), 1008–1019.
- Lesparre, N., Grychtol, B., Gibert, D., Komorowski, J.C., Adler, A., 2014. Cross-section electrical resistance tomography of La Soufrière of Guadeloupe lava dome. *Geophys. J. Int.* 197 (3), 1516–1526.
- López, D.L., Williams, S.N., 1993. Catastrophic volcanic collapse: relation to hydrothermal processes. *Science* 260 (5115), 1794–1796.
- Maruvanchery, V., Kim, E., 2019. Effects of water on rock fracture properties: Studies of mode I fracture toughness, crack propagation velocity, and consumed energy in calcite-cemented sandstone. *Geomech. Eng.* 17 (1), 57–67.
- Mastin, L.G., 1994. Explosive tephra emissions at Mount St. Helens, 1989–1991: the violent escape of magmatic gas following storms? *Geol. Soc. Am. Bull.* 106 (2), 175–185.
- Masuda, K., 2001. Effects of water on rock strength in a brittle regime. *J. Struct. Geol.* 23 (11), 1653–1657.
- Matthews, A.J., Barclay, J., 2004. A thermodynamical model for rainfall-triggered volcanic dome collapse. *Geophys. Res. Lett.* 31 (5).
- Matthews, A.J., Barclay, J., Carn, S., Thompson, G., Alexander, J., Herd, R., Williams, C., 2002. Rainfall-induced volcanic activity onMontserrat. *Geophys. Res. Lett.* 29 (13), 22–1.
- Matthews, A.J., Barclay, J., Johnstone, J.E., 2009. The fast response of volcano-seismic activity to intense precipitation: triggering of primary volcanic activity by rainfall at Soufrière Hills Volcano, Montserrat. *J. Volcanol. Geotherm. Res.* 184 (3–4), 405–415.
- McBirney, A.R., 1955. Thoughts on the eruption of the Nicaraguan Volcano Las Pilas. *Bull. Volcanol.* 17 (1), 113–117.
- McGuire, W.J., 1996. Volcano instability: a review of contemporary themes. *Geol. Soc. Lond. Spec. Publ.* 110 (1), 1–23.
- McKee, C.O., Wallace, D.A., Almond, R.A., Talai, B., 1981. Fatal hydro-eruption of Karkar volcano in 1979: development of a maar-like crater. In: Cooke-Ravian Volume of Volcanological Papers, Vol. 10. Geological Survey of Papua New Guinea, Port Moresby, Papua New Guinea, pp. 63–84.
- Moon, V., Jayawardane, J., 2004. Geomechanical and geochemical changes during early stages of weathering of Karamu Basalt, New Zealand. *Eng. Geol.* 74 (1–2), 57–72.
- Moon, V., Bradshaw, J., de Lange, W., 2009. Geomorphic development of White Island Volcano based on slope stability modelling. *Eng. Geol.* 104 (1–2), 16–30.

- Mordensky, S.P., Villeneuve, M.C., Kennedy, B.M., Heap, M.J., Gravley, D.M., Farquharson, J.I., Reuschlé, T., 2018. Physical and mechanical property relationships of a shallow intrusion and volcanic host rock, Pinnacle Ridge, Mt. Ruapehu, New Zealand. *J. Volcanol. Geotherm. Res.* 359, 1–20.
- Mordensky, S.P., Heap, M.J., Kennedy, B.M., Gilg, H.A., Villeneuve, M.C., Farquharson, J.I., Gravley, D.M., 2019. Influence of alteration on the mechanical behaviour and failure mode of andesite: implications for shallow seismicity and volcano monitoring. *Bull. Volcanol.* 81, 1–12.
- Mordensky, S.P., Villeneuve, M.C., Kennedy, B.M., Struthers, J.D., 2022. Hydrothermally induced edifice destabilisation: the mechanical behaviour of rock mass surrounding a shallow intrusion in andesitic lavas, Pinnacle Ridge, Ruapehu, New Zealand. *Eng. Geol.* 305, 106696.
- Moretti, R., Komorowski, J.C., Ucciani, G., Moune, S., Jessop, D., de Chabalier, J.B., Chaussidon, M., 2020. The 2018 unrest phase at La Soufrière of Guadeloupe (French West Indies) andesitic volcano: Scrutiny of a failed but prodromal phreatic eruption. *J. Volcanol. Geotherm. Res.* 393, 106769.
- Moune, S., Moretti, R., Burtin, A., Jessop, D.E., Didier, T., Robert, V., Buscetti, M., 2022. Gas monitoring of volcanic-hydrothermal plumes in a tropical environment: the case of La Soufrière de Guadeloupe unrest volcano (Lesser Antilles). *Front. Earth Sci.* 10, 17.
- Nara, Y., Morimoto, K., Hiroyoshi, N., Yoneda, T., Kaneko, K., Benson, P.M., 2012. Influence of relative humidity on fracture toughness of rock: implications for subcritical crack growth. *Int. J. Solids Struct.* 49 (18), 2471–2481.
- Nicolas, A., Fortin, J., Regnet, J.B., Dimanov, A., Guéguen, Y., 2016. Brittle and semi-brittle behaviours of a carbonate rock: influence of water and temperature. *Geophys. J. Int.* 206 (1), 438–456.
- Nicollin, F., Gibert, D., Beauducel, F., Boudon, G., Komorowski, J.C., 2006. Electrical tomography of La Soufrière of Guadeloupe Volcano: Field experiments, 1D inversion and qualitative interpretation. *Earth Planet. Sci. Lett.* 244 (3–4), 709–724.
- Noël, C., Baud, P., Violay, M., 2021. Effect of water on sandstone's fracture toughness and frictional parameters: Brittle strength constraints. *Int. J. Rock Mech. Min. Sci.* 147, 104916.
- Norini, G., Bustos, E., Arnosio, M., Baez, W., Zuluaga, M.C., Roverato, M., 2020. Unusual volcanic instability and sector collapse configuration at Chimpa volcano, Central Andes. *J. Volcanol. Geotherm. Res.* 393, 106807.
- Operfelt, S., Delmelle, P., Boivin, P., Delvaux, B., 2006. The 1998 debris avalanche at Casita volcano, Nicaragua: Investigation of the role of hydrothermal smectite in promoting slope instability. *Geophys. Res. Lett.* 33 (15).
- Peruzzetto, M., Komorowski, J.C., Le Friant, A., Rosas-Carbajal, M., Mangeney, A., Legendre, Y., 2019. Modeling of partial dome collapse of La Soufrière of Guadeloupe volcano: implications for hazard assessment and monitoring. *Sci. Rep.* 9 (1), 13105.
- Pola, A., Crosta, G.B., Fusi, N., Castellanza, R., 2014. General characterization of the mechanical behaviour of different volcanic rocks with respect to alteration. *Eng. Geol.* 169, 1–13.
- Potyondy, D.O., Cundall, P.A., 2004. A bonded-particle model for rock. *Int. J. Rock Mech. Min. Sci.* 41 (8), 1329–1364.
- Rad, S.D., Allègre, C.J., Louvat, P., 2007. Hidden erosion on volcanic islands. *Earth Planet. Sci. Lett.* 262 (1–2), 109–124.
- Reid, M.E., 2004. Massive collapse of volcano edifices triggered by hydrothermal pressurization. *Geology* 32 (5), 373–376.
- Reid, M.E., Sisson, T.W., Brien, D.L., 2001. Volcano collapse promoted by hydrothermal alteration and edifice shape, Mount Rainier. *Wash. Geol.* 29 (9), 779–782.
- Reid, M.E., Keith, T.E., Kayen, R.E., Iverson, N.R., Iverson, R.M., Brien, D.L., 2010. Volcano collapse promoted by progressive strength reduction: new data from Mount St. Helens. *Bull. Volcanol.* 72, 761–766.
- Risnes, R., Madland, M.V., Hole, M., Kwabiah, N.K., 2005. Water weakening of chalk—Mechanical effects of water-glycol mixtures. *J. Pet. Sci. Eng.* 48 (1–2), 21–36.
- Rodell, M., Velicogna, I., Famiglietti, J.S., 2009. Satellite-based estimates of groundwater depletion in India. *Nature* 460 (7258), 999–1002.
- Rodríguez, A., van Bergen, M.J., 2017. Superficial alteration mineralogy in active volcanic systems: an example of Poás volcano, Costa Rica. *J. Volcanol. Geotherm. Res.* 346, 54–80.
- Romero, J.E., Polacci, M., Watt, S., Kitamura, S., Tormey, D., Sielfeld, G., Polanco, E., 2021. Volcanic lateral collapse processes in mafic arc edifices: a review of their driving processes, types and consequences. *Front. Earth Sci.* 9, 639825.
- Rosas-Carbajal, M., Komorowski, J.C., Nicollin, F., Gibert, D., 2016. Volcano electrical tomography unveils edifice collapse hazard linked to hydrothermal system structure and dynamics. *Sci. Rep.* 6 (1), 29899.
- Rosas-Carbajal, M., Jourde, K., Marteau, J., Deroussi, S., Komorowski, J.C., Gibert, D., 2017. Three-dimensional density structure of La Soufrière of Guadeloupe lava dome from simultaneous muon radiographies and gravity data. *Geophys. Res. Lett.* 44 (13), 6743–6751.
- Rouwet, D., Tassi, F., Mora-Amador, R., Sandri, L., Chiarini, V., 2014. Past, present and future of volcanic lake monitoring. *J. Volcanol. Geotherm. Res.* 272, 78–97.
- Rutter, E.H., Mainprice, D.H., 1978. The effect of water on stress relaxation of faulted and unfaulted sandstone. *Rock Fract. Earthq. Predict.* 634–654.
- Sahoo, S., Tiwari, D.K., Panda, D., Kundu, B., 2022. Eruption cycles of Mount Etna triggered by seasonal climatic rainfall. *J. Geodyn.* 149, 101896.
- Salaün, A., Villemant, B., Gérard, M., Komorowski, J.C., Michel, A., 2011. Hydrothermal alteration in andesitic volcanoes: trace element redistribution in active and ancient hydrothermal systems of Guadeloupe (Lesser Antilles). *J. Geochem. Explor.* 111 (3), 59–83.
- Sammis, C.G., Ashby, M.F., 1986. The failure of brittle porous solids under compressive stress states. *Acta Metall.* 34 (3), 511–526.
- Saucedo, R., Macías, J.L., Sarocchi, D., Bursik, M., Rupp, B., 2008. The rain-triggered Atenuique volcaniclastic debris flow of October 16, 1955 at Nevado de Colima Volcano, Mexico. *J. Volcanol. Geotherm. Res.* 173 (1–2), 69–83.
- Schaefer, L.N., Oommen, T., Corazzato, C., Tibaldi, A., Escobar-Wolf, R., Rose, W.I., 2013. An integrated field-numerical approach to assess slope stability hazards at volcanoes: the example of Pacaya, Guatemala. *Bull. Volcanol.* 75, 1–18.
- Schaefer, L.N., Kereszturi, G., Kennedy, B.M., Villeneuve, M., 2023. Characterizing lithological, weathering, and hydrothermal alteration influences on volcanic rock properties via spectroscopy and laboratory testing: a case study of Mount Ruapehu volcano, New Zealand. *Bull. Volcanol.* 85 (8), 43.
- Scher, S., Williams-Jones, A.E., Williams-Jones, G., 2013. Fumarolic activity, acid-sulfate alteration, and high sulfidation epithermal precious metal mineralization in the crater of Kawah Ijen Volcano, Java, Indonesia. *Econ. Geol.* 108 (5), 1099–1118.
- Schmitt, L., Forsans, T., Santarelli, F.J., 1994. Shale testing and capillary phenomena. *Int. J. Rock Mech. Min. Sci. Geomech. Abstr.* 31 (5), 411–427.
- Sens-Schönfelder, C., Wegler, U., 2006. Passive image interferometry and seasonal variations of seismic velocities at Merapi Volcano, Indonesia. *Geophys. Res. Lett.* 33 (21).
- Siebert, L., Glicken, H., Ui, T., 1987. Volcanic hazards from Bezymianny-and Bandai-type eruptions. *Bull. Volcanol.* 49, 435–459.
- Simmons, J., Elsworth, D., Voight, B., 2004. Instability of exogenous lava lobes during intense rainfall. *Bull. Volcanol.* 66, 725–734.
- Singh, T.N., Singh, S.K., Mishra, A., Singh, P.K., Singh, V.K., 1999. Effect of acidic water on physico-mechanical behaviour of rock. *Indian J. Eng. Mater. Sci.* 6, 66–72.
- Tamburello, G., Moune, S., Allard, P., Venugopal, S., Robert, V., Rosas-Carbajal, M., Moretti, R., 2019. Spatio-temporal relationships between fumarolic activity, hydrothermal fluid circulation and geophysical signals at an arc volcano in degassing unrest: La Soufrière of Guadeloupe (French West Indies). *Geosciences* 9 (11), 480.
- Tang, S.B., Yu, C.Y., Heap, M.J., Chen, P.Z., Ren, Y.G., 2018. The influence of water saturation on the short-and long-term mechanical behavior of red sandstone. *Rock Mech. Rock. Eng.* 51, 2669–2687.
- Tanguy, J.-C., 1994. The 1902–1905 eruptions of Montagne Pelée, Martinique: anatomy and retrocession. *J. Volcanol. Geotherm. Res.* 60, 87–107.
- Taron, J., Elsworth, D., Thompson, G., Voight, B., 2007. Mechanisms for rainfall-concurrent lava dome collapses at Soufrière Hills Volcano, 2000–2002. *J. Volcanol. Geotherm. Res.* 160 (1–2), 195–209.
- Tost, M., Cronin, S.J., 2016. Climate influence on volcano edifice stability and fluvial landscape evolution surrounding Mount Ruapehu, New Zealand. *Geomorphology* 262, 77–90.
- Uralab, M., Petersen, F., Gross, F., Bonforte, A., Puglisi, G., Guglielmino, F., Kopp, H., 2018. Gravitational collapse of Mount Etna's southeastern flank. *Sci. Adv.* 4 (10), eaat9700.
- van Hinsberg, V., Berlo, K., van Bergen, M., Williams-Jones, A., 2010. Extreme alteration by hyperacidic brines at Kawah Ijen volcano, East Java, Indonesia: I. Textural and mineralogical imprint. *J. Volcanol. Geotherm. Res.* 198 (1–2), 253–263.
- van Wyk de Vries, B., Francis, P.W., 1997. Catastrophic collapse at stratovolcanoes induced by gradual volcano spreading. *Nature* 387 (6631), 387–390.
- van Wyk de Vries, B., Kerle, N., Petley, D., 2000. Sector collapse forming at Casita volcano, Nicaragua. *Geology* 28 (2), 167–170.
- Vazquez, R., Macias, J.L., Alcala-Reygoza, J., Arce, J.L., Jimenez-Haro, A., Fernandez, S., Sanchez-Nunez, J.M., 2022. Numerical modeling and hazard implications of landslides at the Ardillas Volcanic Dome (Tacana Volcanic Complex, Mexico-Guatemala). *Nat. Hazards* 113 (2), 1305–1333.
- Villemant, B., Hammouya, G., Michel, A., Semet, M.P., Komorowski, J.C., Boudon, G., Cheminée, J.L., 2005. The memory of volcanic waters: shallow magma degassing revealed by halogen monitoring in thermal springs of La Soufrière volcano (Guadeloupe, Lesser Antilles). *Earth Planet. Sci. Lett.* 237 (3–4), 710–728.
- Villemant, B., Komorowski, J.-C., Dessert, C., Michel, A., Crispì, O., Hammouya, G., Beauducel, F., Chabalier, D., 2014. Evidence for a new shallow magma intrusion at La Soufrière of Guadeloupe (Lesser Antilles). Insights from long-term geochemical monitoring of halogen-rich hydrothermal fluids. *J. Volcanol. Geotherm. Res.* 285, 247–277.
- Violette, S., De Marsily, G., Carbonnel, J.P., Goblet, P., Ledoux, E., Tijani, S.M., Vouillé, G., 2001. Can rainfall trigger volcanic eruptions? A mechanical stress model of an active volcano: 'Piton de la Fournaise', Reunion Island. *Terra Nova* 13 (1), 18–24.
- Voight, B., Glicken, H., Janda, R.J., Douglass, P.M., 1981. Catastrophic rockslide avalanche of May 18. In: Lipman, P.W., Mullineaux, D.R. (Eds.), *The 1980 Eruptions of Mount St. Helens, Washington, US Geological Survey, Professional Papers*, 1250, pp. 347–378.
- Voight, B., Komorowski, J.C., Norton, G.E., Belousov, A.B., Belousova, M., Boudon, G., Francis, P.W., Franz, W., Heinrich, P., Sparks, R.S.J., Young, S.R., 2002. The 1997 Boxing Day Sector Collapse and Debris Avalanche, Soufrière Hills Volcano, Montserrat, W.I. In: Druitt, T.H., Kokelaar, B.P. (Eds.), *The eruption of Soufrière Hills Volcano, Montserrat, from 1995 to 1999*, Geological Society, London Memoirs, 21, pp. 363–407.
- Wallace, C.S., Schaefer, L.N., Villeneuve, M.C., 2022. Material properties and triggering mechanisms of an andesitic lava dome collapse at Shiveluch Volcano, Kamchatka, Russia, revealed using the finite element method. *Rock Mech. Rock. Eng.* 55 (5), 2711–2728.
- Walter, T.R., Zorn, E.U., Harnett, C.E., Shevchenko, A.V., Belousov, A., Belousova, M., Vassileva, M.S., 2022. Influence of conduit and topography complexity on spine extrusion at Shiveluch volcano, Kamchatka. *Commun. Earth Environ.* 3 (1), 169.
- Wang, J.J., Zhu, J.G., Chiu, C.F., Zhang, H., 2007. Experimental study on fracture toughness and tensile strength of a clay. *Eng. Geol.* 94 (1–2), 65–75.

- Wasantha, P.L., Ranjith, P.G., 2014. Water-weakening behavior of Hawkesbury sandstone in brittle regime. *Eng. Geol.* 178, 91–101.
- Watters, R.J., Zimbelman, D.R., Bowman, S.D., Crowley, J.K., 2000. Rock mass strength assessment and significance to edifice stability, Mount Rainier and Mount Hood, Cascade Range volcanoes. *Pure Appl. Geophys.* 157, 957–976.
- Wyering, L.D., Villeneuve, M.C., Wallis, I.C., Siratovich, P.A., Kennedy, B.M., Gravley, D.M., Cant, J.L., 2014. Mechanical and physical properties of hydrothermally altered rocks, Taupo Volcanic Zone, New Zealand. *J. Volcanol. Geotherm. Res.* 288, 76–93.
- Yamasato, H., Kitagawa, S., Komiya, M., 1998. Effect of rainfall on dacitic lava dome collapse at Unzen volcano, Japan. *Pap. Meteorol. Geophys.* 48 (3), 73–78.
- Yilmaz, T.I., Wadsworth, F.B., Gilg, H.A., Hess, K.U., Kendrick, J.E., Wallace, P.A., Dingwell, D.B., 2021. Rapid alteration of fractured volcanic conduits beneath Mt Unzen. *Bull. Volcanol.* 83, 1–14.
- Young, S., Voight, B., Barclay, J., Herd, R.A., Komorowski, J.-C., Miller, A.D., Sparks, R.S., Stewart, R.C., 2002. Hazard implications of small-scale edifice instability and sector collapse: a case history from Soufrière Hills volcano, Montserrat. In: Druitt, T.H., Kokelaar, B.P. (Eds.), *The eruption of Soufrière Hills Volcano, Montserrat, from 1995 to 1999*, Geological Society, London, Memoirs, 21, pp. 349–361.
- Zhu, W., Baud, P., Wong, T.F., 2010. Micromechanics of cataclastic pore collapse in limestone. *J. Geophys. Res. Solid Earth* 115 (B4).
- Zhu, W., Baud, P., Vinciguerra, S., Wong, T.F., 2011. Micromechanics of brittle faulting and cataclastic flow in Alban Hills tuff. *J. Geophys. Res. Solid Earth* 116 (B6).
- Zhu, W., Baud, P., Vinciguerra, S., Wong, T.F., 2016. Micromechanics of brittle faulting and cataclastic flow in Mount Etna basalt. *J. Geophys. Res. Solid Earth* 121 (6), 4268–4289.
- Zimbelman, D.R., 1996. Hydrothermal alteration and its influence on volcanic hazards—Mount Rainier, Washington, a case history. University of Colorado at Boulder.
- Zimbelman, D.R., Rye, R.O., Breit, G.N., 2005. Origin of secondary sulfate minerals on active andesitic stratovolcanoes. *Chem. Geol.* 215 (1–4), 37–60.